Physica Scripta

PAPER

Tailoring the physical characteristics of $ScTaPd_2Sn_2$ and $ScTaPt_2Sn_2$ double half-Heusler compound for thermoelectric applications

H Mekki[1,2], H Baaziz[1,2], Z Charifi[1,2], T Ghellab[1,2] and I Mili[2]

[1] Department of Physics, Faculty of Science, University of M'sila, 28000 M'sila, Algeria
[2] Laboratory of physics and chemistry of materials, University of M'sila, Algeria

E-mail: baaziz_hakim@yahoo.fr

Keywords: DHH, optoelectronic, mechanic behaviour, ZT

RECEIVED
9 April 2024

REVISED
28 May 2024

ACCEPTED FOR PUBLICATION
12 June 2024

PUBLISHED
21 June 2024

Abstract

Due to its potential uses in thermoelectrics, spintronics, and other sectors, double half-Heusler compounds have recently attracted much attention. This study presents the first-ever report on the structural, electronic, optical, elastic, and thermoelectric characteristics of the double half Heusler (DHH) compounds $ScTaPd_2Sn_2$ and $ScTaPt_2Sn_2$, employing density functional theory (DFT). Using the EV-GGA approximation, the estimated band structures exhibit a semiconductor behavior with an indirect bandgap of 0.549 eV and 0.851 eV, respectively. In addition, we examined optical characteristics. Our material structural stability and stiffness were confirmed using elastic characteristics. Boltzmann's semiclassical theory attempts to explain a simulation concept in the BoltzTrap software. According to the thermoelectric investigation, these DHH are a p-type material, a candidate for thermoelectric application, specifically when doped.

1. Introduction

In a recent study, Anand *et al* proposed the notion of double half-Heusler (DHH) compounds characterized by their enhanced structural complexity, which leads to substantially reduced K_L values, this novel group of half Heusler alloys exhibits many chemical formulas, including double quaternary ($X'X''Y_2Z_2$; $X_2Y'Y''Z_2$; $X_2Y_2Z'Z''$), triple ($X_2'X''Y_3Z_3$), and quadruple ($X'_3X''Y_4Z_4$) [1]. In the context of this investigation, a significant focal point pertains to the quaternary double half Heusler compounds, which exhibit analogous characteristics. These characteristics encompass behaviors to semiconductors, an indirect and narrow band gap, a substantial contribution to the density of states from the d-orbital, mechanical stability, and a Debye temperature of approximately 400 K [2–6]. Furthermore, the researchers Anand *et al* conducted an experimental study to showcase the reduced thermal conductivity (K_L) of the compound $Ti_2FeNiSb_2$, which was synthesized by combining the aliovalent compounds TiFeSb and TiNiSb. The K_L value of $Ti_2FeNiSb_2$ was found to be significantly lower (6–7 W mK^{-1}) compared to that of the compound TiCoSb (25 W mK^{-1}). This reduction in K_L can be attributed to the decreased velocity of phonon groups in the high-frequency range. The recent finding [7] simulated thermal conductivity values of Hf_2Ni_2InSb in its cubic phase range from 13.3 to 3.3 (W mK^{-1}), while in its tetragonal phase, the range is from 12.4 to 2.8 (W mK^{-1}). On the other hand, for the ternary compound HfNiSn, the thermal conductivity ranges from 18.9 to 4.7 (W mK^{-1}) within the temperature range of 300–900 K. The thermal conductivity, denoted as K_L, of Zr_2Ni_2InSb exhibits a range of values between 17.8 to 4.3 (W mK^{-1}) in the cubic crystal structure and 12.1 to 2.9 (W mK^{-1}) in the tetragonal crystal structure throughout the temperature range of 300–900 K. In comparison, the thermal conductivity of ZrNiSn within the same temperature range varies between 18.7 to 4.5 (W mK^{-1}). The previously reported thermal conductivity values at ambient temperature for ZrNiSn and HfNiSn are 19.6 and 18.5 (W mK^{-1}), respectively. In contrast, for Zr_2Ni_2InSb and Hf_2Ni_2InSb in the tetragonal phase, the corresponding values at 300 K are 13.5 and 12.5 (W mK^{-1}), respectively at 300 K [1]. Another illustration from the research we've done in previous periods about the DHH $ScNbNi_2Sn_2$ which has a lower K_L 5.3 (W mK^{-1}). At 300 K and 1.3 (W mK^{-1}) at 1000 K [2] however, a parent ScNiSn has 11.7 (W mK^{-1}) at 300 K [8]

Half-Heusler compounds can be synthesised using a diverse range of elements, wherein each lattice site accommodates a distinct group of elements. Based on the valence balance rule [9], it is expected that the net valence (NV) of the three components in stable compounds should be zero. Therefore, this criterion can be used to choose from the different possible ternary half-Heusler compounds (generally XYZ) based on their constituent elements. Several alloy compositions form disordered solutions that can only be sustained at high temperatures. The stability of double half-Heusler materials ($X_2Y'Y''Z_2$ instead of XYZ, with Y′ and Y″ being non-isovalent) is established via aliovalent replacement. This notion is derived from the idea of double perovskites, where the term 'double' signifies the duplication of the perovskite formula unit ($A_2B'B'O_6$ as compared to ABO_3). The materials that exhibit aliovalent substitution, such as $ScNbNi_2Sn_2$, are commonly referred to as double half-Heusler compounds. This nomenclature is used to distinguish them from other quaternary configurations that are alloyed isovalently regardless of whether they experience an order–disorder transformation at elevated temperatures or not. In contrast to ternary compositions, the inclusion of quaternary elements in double half-Heusler structures offers a significantly larger phase space for the exploration and discovery of new compounds.

Our study aims to analyze the electronic properties of $ScTaPd_2Sn_2$ and $ScTaPt_2Sn_2$, specifically their band structure and density of states (DOS). Additionally, we seek to investigate its thermoelectric properties, particularly the Seebeck coefficient. The outcomes of electrical conductivity, electronic thermal conductivity, the Seebeck coefficient, and the figure of merit are presented alongside an explanation of the computational framework derived from Boltzmann's semiclassical theory, utilizing the BoltzTrap code. Moreover, the elastic and optical properties are presented in the last part of the article. However, there seems to be a scarcity of similar inquiries in the existing body of literature.

The objective of our research is to analyse the electrical properties of $ScTaPd_2Sn_2$ and $ScTaPt_2Sn_2$, specifically their band structure and density of states (DOS). Additionally, we seek to investigate their thermoelectric capabilities, particularly their Seebeck value. The computational model described in Boltzmann's semiclassical theory is utilised to determine the electrical conductivity, electronic thermal conductivity, Seebeck coefficient, and figure of merit. Moreover, the optical properties such as the dielectric function and optical conductivity are determined. Nevertheless, there is a lack of comparable studies in the existing body of literature.

The manuscript is divided into four sections, with the opening portion providing a detailed analysis of the importance and practical uses of DHH. The second section provides an explanation of the approach or computational details. Within the third section, we will proceed to showcase our findings. The final section presents the conclusions drawn from all the results.

2. Computation details

The Wien2k code [10, 11] implements the full linearized augmented plane wave (FP-LAPW) method [12], which relies on density functional theory, or DFT [13]. In our research, we utilize the generalized gradient approximation (GGA-PBE) [14] and the local density approximation (LDA) [15] to handle the exchange–correlation energy. Additionally, we incorporate the modified Beck-Johnson [16] and the Engel-Vosko (EV-GGA) [17] potentials to enhance the accuracy of the electronic structure. The muffin-tin radius (R.M.T) for $ScTaPd_2Sn_2$ varies between 2.31 and 2.37 atomic units (a.u.), while for $ScTaPt_2Sn_2$ it varies between 2.26 to 2.37 a.u. The highest modulus of the reciprocal vector K_{max} is found in the first *Brillouin zone*. To establish a relationship, we equate the product of R.M.T $\times$ K_{max} to 9. The wave function expansion parameters within the muffin tin are $l_{max} = 10$ and $G_{max} = 12$. G_{max} represents the magnitude of the largest vector in the Fourier expansion of the charge density. By including 1000 and 900 k-points for $ScTaPd_2Sn_2$ and $ScTaPt_2Sn_2$ respectively in the Brillouin zone, the computations are ensured to be precise. The self-consistent computation is said to have reached convergence when the total energy difference is 10^{-4} Ry. The Boltztrap software [18], which is based on the semi-classical Boltzmann theory, is utilized to assess thermoelectric transport properties. Additionally, the impact of temperature and pressure on the Debye temperature and lattice thermal expansion is estimated using the quasi-harmonic approximation integrated in the Gibbs software [19, 20].

3. Result and analysis

3.1. Structural properties

The arrangement of atoms or molecules in a material determines its structural properties. These properties can be divided into geometrical properties, which include crystal structure, and lattice parameters, and we can predict physical properties such as electronic, optical, elastic, and thermoelectric based on geometrical properties. Our double half-Heusler $ScTaSn_2Pd_2$ and $ScTaPt_2Sn_2$ alloys structural characteristics are examined in this section.

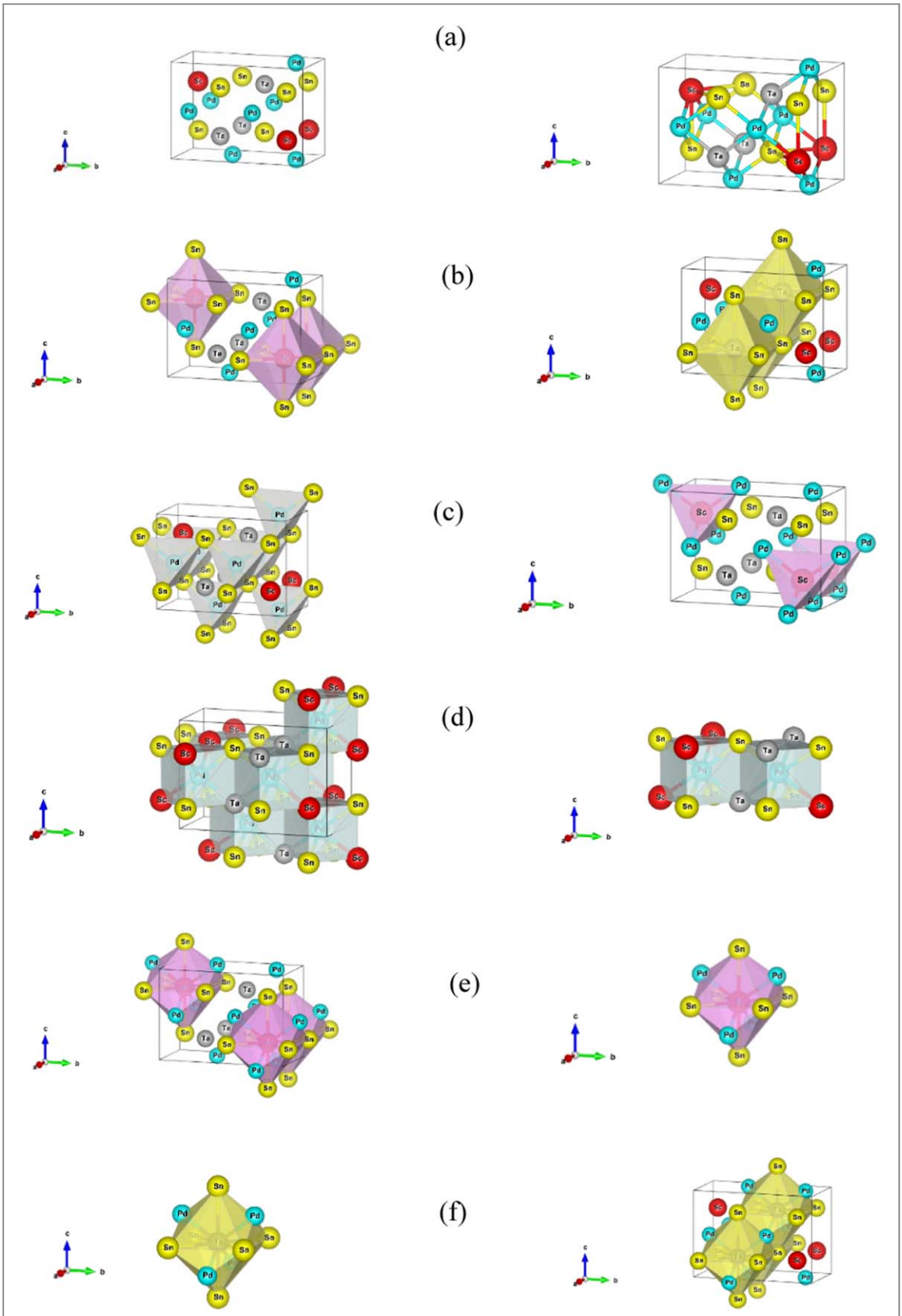

Figure 1. Crystal structure of the double half-Heusler $ScTaPd_2Sn_2$ compound (a) Conventional unit cell, (b) the octahedral $X'Z_6$, XZ_6, (c) the tetrahedral YZ_4, XY_4 (d) cube YXX'_3Z_3, $YX_3X'Z_3$ (e)and (f) bicapped square prism XY_4Z_6, $X'Y_4Z_6$ according to the direction (111).

$ScTaPd_2Sn_2$ and $ScTaPt_2Sn_2$ is half-Heusler-derived structured and crystallize in the simple orthorhombic with the space group $Pmn2_1$ (N°31). The structures depicted in figure 1 is referred to as double half-Heusler structures, which are formed by combining two half-Heusler compounds with a distinct crystal arrangement. In

Table 1. The positions of atoms in the DHH of $ScTaPd_2Sn_2$ and $ScTaPt_2Sn_2$.

Compound	Atom	x (Bohr)	y	z
$ScTaPd_2Sn_2$	Sc	0.50000000	0.12166132	0.75504239
		0.00000000	0.87833868	0.25594239
	Ta	0.00000000	0.37356296	0.26112829
		0.50000000	0.62643704	0.76112829
	Sn1	0.50000000	0.62678591	0.26624628
		0.00000000	0.37321409	0.76624628
	Sn2	0.00000000	0.87488038	0.75024701
		0.50000000	0.12511962	0.25024701
	Pd1	0.00000000	0.13462731	0.50000000
		0.50000000	0.86537269	0.00000000
	Pd2	0.00000000	0.61538705	0.51745290
		0.50000000	0.38461295	0.01745290
$ScTaPt_2Sn_2$	Sc	0.50000000	0.62243198	0.26900163
		0.00000000	0.37756802	0.76900163
	Ta	0.00000000	0.87556905	0.75938957
		0.50000000	0.12443095	0.25938957
	Sn1	0.00000000	0.37796990	0.27383598
		0.50000000	0.62203010	0.77383598
	Sn2	0.50000000	0.13007003	0.75178726
		0.00000000	0.86992997	0.25178726
	Pt1	0.00000000	0.11402053	0.50000000
		0.50000000	0.88597947	0.00000000
	Pt2	0.00000000	0.63662292	0.52598238
		0.50000000	0.36337708	0.02508238

Table 2. Calculated structural parameters(A^0) and magnetic moment (μ_B) for $ScTaPd_2Sn_2$ and $ScTaPt_2Sn_2$ compounds using GGA and LDA approximations.

Compounds 31_Pmn21	App	a(A^0)	b	c	b/a	c/a	E_{min} (Ryd)	B(GPa)	B‘	M_{Tot} (μ_B)
$ScTaPd_2Sn_2$	GGA	4.4029	8.8386	6.2475	2.0074	1.4188	−155307.887786	135.0660	4.8254	0.00054
	LDA	4.3655	8.7636	6.1935	2.0074	1.4188	−155307.887760	145.0508	4.9720	0.00034
$ScTaPt_2Sn_2$	GGA	4.4245	8.8617	6.2658	2.0028	1.4161	−262483.766381	152.8098	5.0062	−0.00033
	LDA	4.3975	8.8076	6.2276	2.0028	1.4161	−262400.542383	162.7297	5.0974	0.00139

order to produce completely stable geometrical configurations of the DHH alloys, we extensively optimized the atomic structure by relaxing the cell parameters. The relaxed atomic coordinates discovered are shown in table 1. In order to establish the equilibrium lattice constant and define the stable structure of the examined double half-Heusler alloy, structural optimizations on the $ScTaPd_2Sn_2$ alloy for ferromagnetic (FM) and paramagnetic (PM) phases are also carried out. The total energy values can be adjusted as a function of volume by employing the Birch-Murnaghan equation of state (EOS) [21] in conjunction with the LDA and GGA approximations.

Table 2 shows the optimized results for the lattice parameter a, bulk modulus B (GPa), and its first derivative B′. Based on the current findings shown in table 2, the calculated optimized b/a and c/a ratios were 2.0074 and 1.4188 for $ScTaPd_2Sn_2$, 2.0028,1.4161 for $ScTaPt_2Sn_2$ and 2.0074/2.0073 in the context of GGA approximation. The aforementioned values suggest a marginal deformation of both compounds. By transitioning from the GGA to the LDA approximation, it becomes apparent that the bulk modulus increases while the lattice parameters a and b decrease. Additionally, the substitution of atoms Pd with Pt causes an increase in the aforementioned parameters. Since $ScTaPt_2Sn2$ has a greater modulus of compressibility than $ScTaPd_2Sn_2$, it is incompressible in comparison to $ScTaPd_2Sn_2$.

According to figure 2, Sc is bonded in a 10-coordinate geometry Sc is attached to four Pd and six Sn atoms to form distorted face -sharing $ScPd_4Sn_6$ tetrahedra Sc-Pd lengths chemical bonds are divided into tree shorter (2.72001Å) and one longer (2.84417Å). Three shorter (3.09396Å) and three longer (3.12966Å) bond lengths of Sc–Sn, furthermore we delete the Sc-Pd bond we get octahedral site $ScSn_6$ .to form the distorted face sharing $TaPd_4Sn_6$ tetrahedra Ta is bonded to four Pd and six Sn atoms, four Ta-Pd lengths chemical bonds one is shorter (2.58594Å) and three longer (2.67836Å) (see table 1). Four Ta-Sn bond lengths three are shorter (3.11014Å) and three longer (3.13954Å) Nb–Sn. Two incompatible Pd sites wich shape a body centered cubic geometry to each Sc, Ta, Sn. In the first Pd site, Pd is bonded to one Sc, three equivalent Ta, and four Sn atoms. Four Pd–Sn bonds

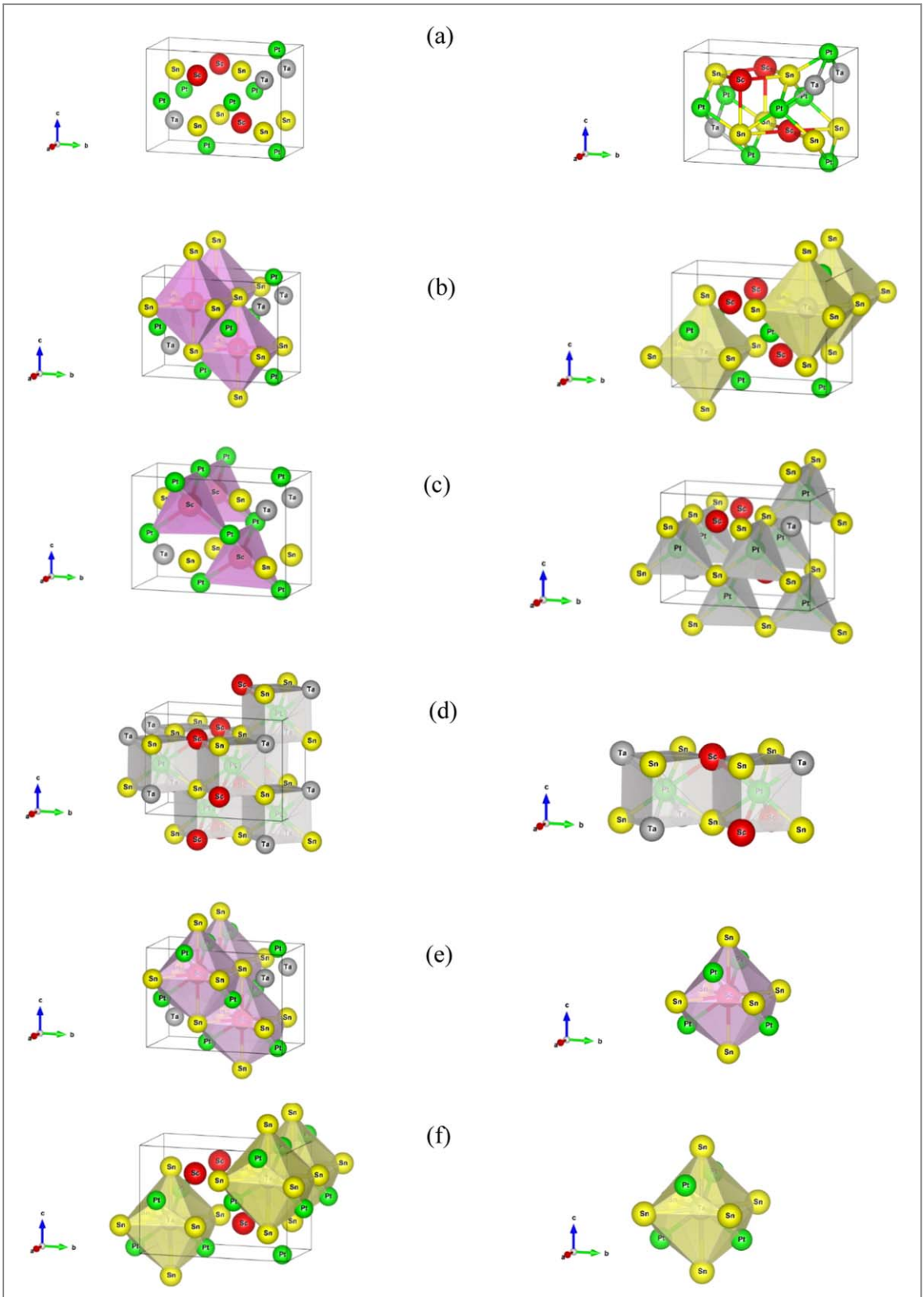

Figure 2. Crystal structure of the double half-Heusler $ScTaPt_2Sn_2$ compound (a) Conventional unit cell, (b) the octahedral $X'Z_6$, XZ_6, (c) the tetrahedral YZ_4, XY_4 (d) cube YXX'_3Z_3,$YX_3X'Z_3$ (e) and (f) bicapped square prism XY_4Z_6,$X'Y_4Z_6$ according to the direction (111).

one is shorter (2.64530 Å) and three longer (2.70 Å). In terms of the second Pd site, we note that Pd is bonded to three Sc, one Ta, and four Sn atoms. Four Pd–Sn bonds, three are shorter (2.69Å) and one longer (2.77 Å). for the Tin atom has two distinct sites. In the first Sn site, Sn is connected in 10 coordinates to three equivalent Sc, three equivalent Ta, and four Pd atoms. For the second Sn atom, Sn has 10-coordinate 3 Sc, 3 Ta, and 4 Pd atoms.

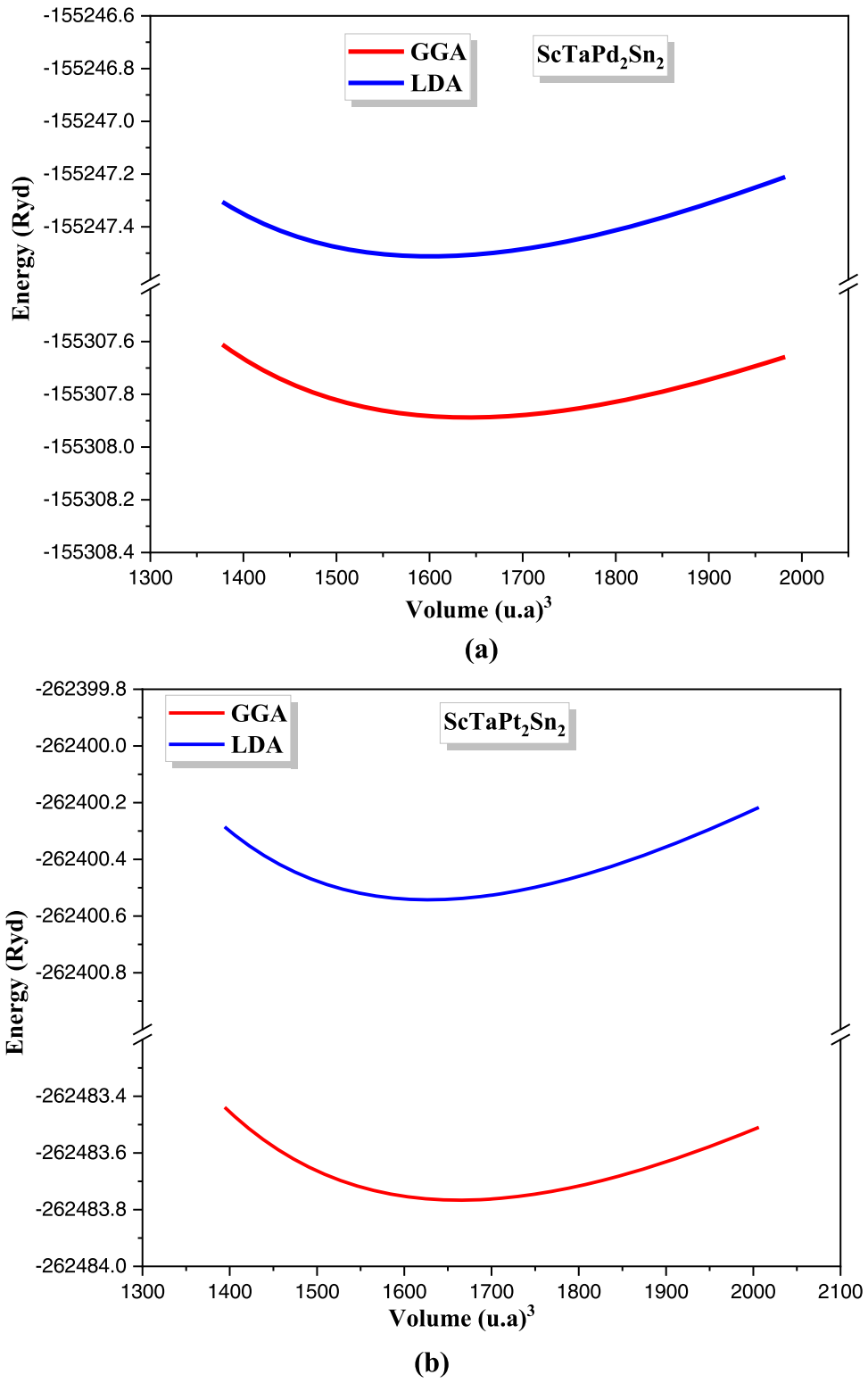

Figure 3. Total energy as a function of volume for (a) $ScTaPd_2Sn_2$ and (b) $ScTaPt_2Sn_2$ compounds using GGA and LDA.

As an example, consider the interatomic distance Sc-Sn1 3.12Å (3.1Å) in $ScTaPd_2Sn_2$ which indicates quite similarities to $ScNbNi_2Sn_2$ using GGA and LDA, respectively (see table 3).

To precisely explain the structural properties of our DHH compounds, we optimized a computation employing two distinct approximations GGA and LDA. Based on figure 3, it appears that the GGA approximation has the lowest energy for both $ScTaPd_2Sn_2$ and $ScTaPt_2Sn_2$, thus we will finish our investigation with it. The calculations indicated that our DHH compounds would exhibit a paramagnetic (PM) state see figure 4.

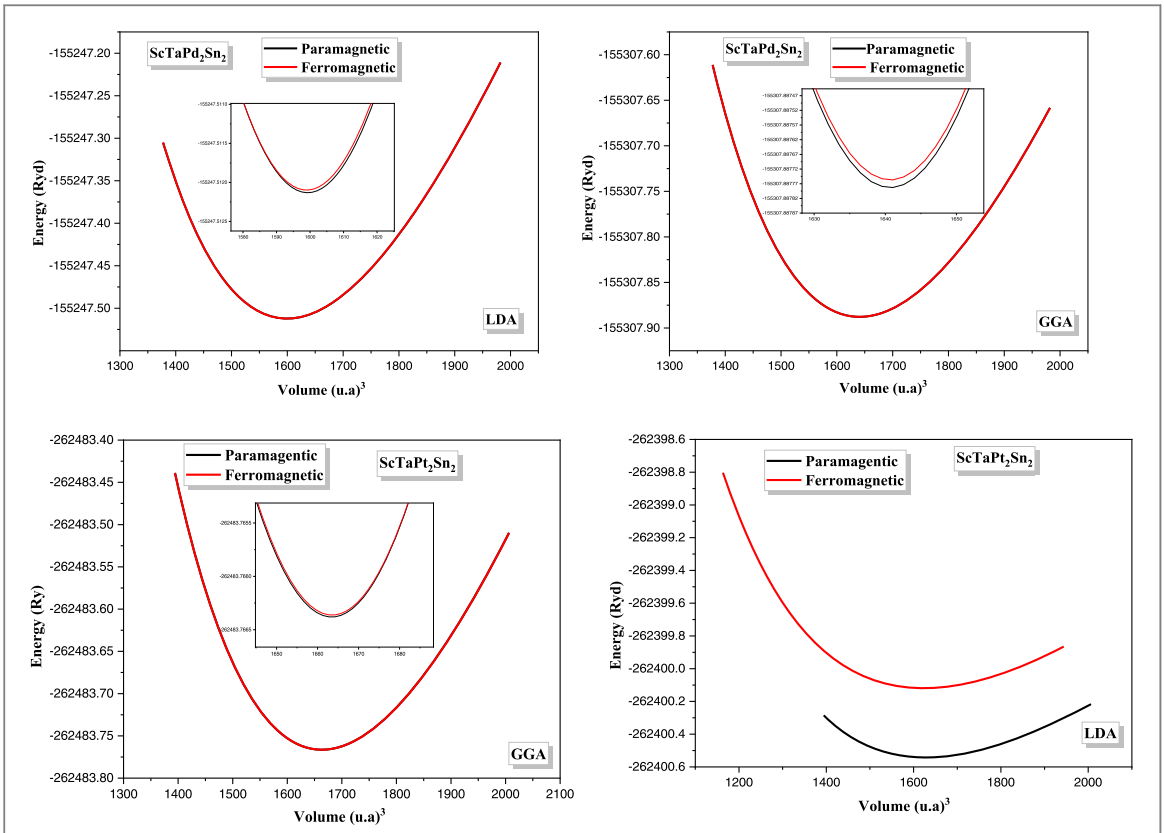

Figure 4. Energy versus unit cell volume in the Paramagnetic and Ferromagnetic configurations of *$ScTaPd_2Sn_2$ and $ScTaPt_2Sn_2$ compounds using GGA and LDA*.

Table 3. Interatomic distances (Å) of $ScTaPd_2Sn_2$, and $ScTaPt_2Sn_2$ DHH compounds using GGA and LDA approximations.

Compounds	Interatomic distance (A^0)	GGA	LDA
$ScTaPd_2Sn_2$	$\mathbf{d_{Sc\text{-}Pd1}}$	2.72001 (x3)	2.69844 (x3)
	$\mathbf{d_{Sc\text{-}Pd2}}$	2.84417 (x1)	2.83635 (x1)
	$\mathbf{d_{Sc\text{-}Sn1}}$	3.12966 (x3)	3.10531 (x3)
	$\mathbf{d_{Sc\text{-}Sn2}}$	3.09396 (x3)	3.06744 (x3)
	$\mathbf{d_{Ta\text{-}Pd1}}$	2.58594 (x1)	2.55564 (x1)
	$\mathbf{d_{Ta\text{-}Pd2}}$	2.67836 (x3)	2.65271 (x3)
	$\mathbf{d_{Ta\text{-}Sn1}}$	3.13954 (x3)	3.10793 (x3)
	$\mathbf{d_{Ta\text{-}Sn2}}$	3.11014 (x3)	3.08592 (x3)
	$\mathbf{d_{Sn\text{-}Pd1}}$	2.69 (x3); 2.77 (x1)	2.67 (x3); 2.76 (x1)
	$\mathbf{d_{Sn\text{-}Pd2}}$	2.70 (x3); 2.64 (x1)	2.68 (x3); 2.61 (x1)
$ScTaPt_2Sn_2$	$\mathbf{d_{Sc\text{-}Pt1}}$	2.883 (x1)	2.863 (x1)
	$\mathbf{d_{Sc\text{-}Pt2}}$	2.742 (x3)	2.723 (x3)
	$\mathbf{d_{Sc\text{-}Sn1}}$	3.099 (x3)	3.077 (x3)
	$\mathbf{d_{Sc\text{-}Sn2}}$	3.120 (x3)	3.099 (x3)
	$\mathbf{d_{Ta\text{-}Pt1}}$	2.68 (x3)	2.66 (x3)
	$\mathbf{d_{Ta\text{-}Pt2}}$	2.576 (x1)	2.55 (x1)
	$\mathbf{d_{Ta\text{-}Sn1}}$	3.157 (x3)	3.135 (x3)
	$\mathbf{d_{Ta\text{-}Sn2}}$	3.163 (x3)	3.139 (x3)
	$\mathbf{d_{Sn\text{-}Pt1}}$	2.72 (x3) ; 2.66 (x1)	2.70 (x3); 2.64 (x1)
	$\mathbf{d_{Sn\text{-}Pt2}}$	2.70 (x3); 2.69 (x1)	2.68 (x1); 2.77 (x1)

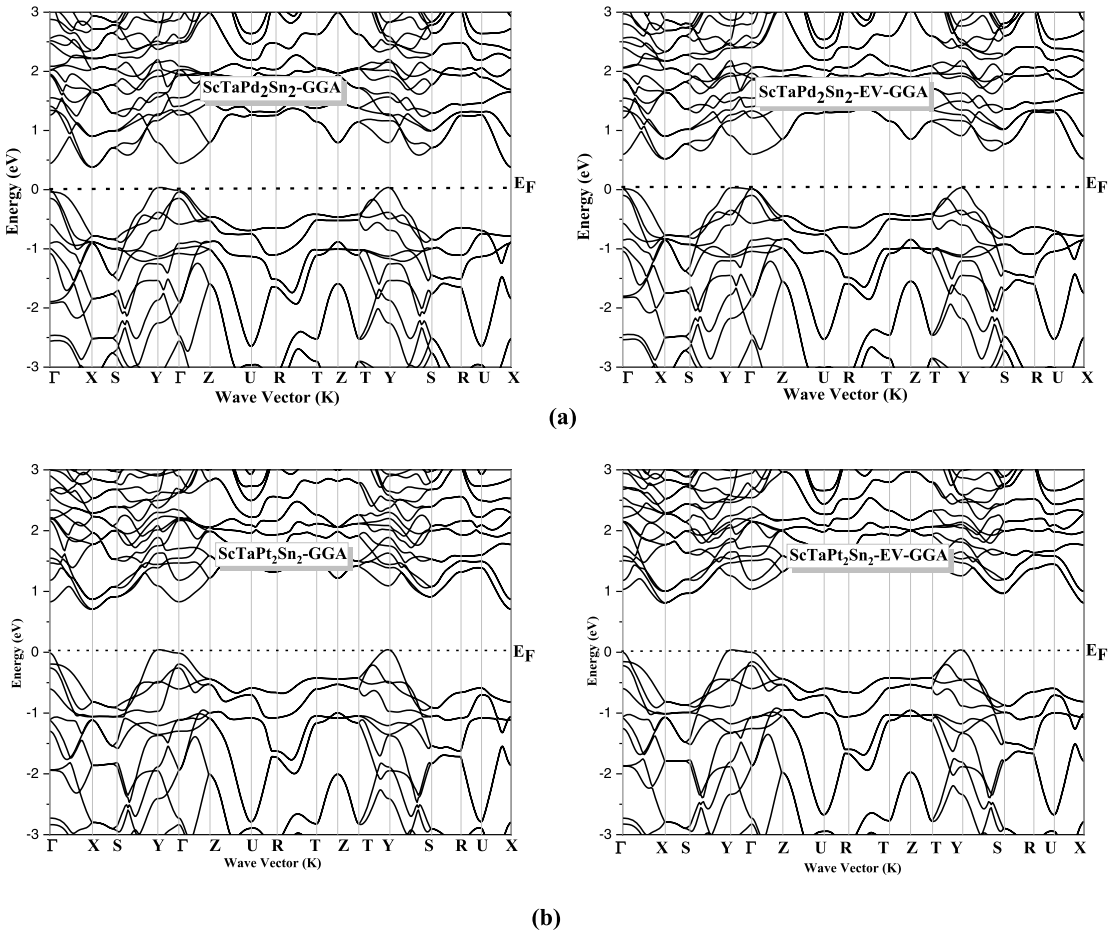

Figure 5. The band structure along the symmetry lines of the BZ of DHH (a) $ScTaPd_2Sn_2$ and (b) $ScTaPt_2Sn_2$ with GGA and EV-GGA.

Table 4. Band gap of $ScTaSn_2Pd_2$ and ScTa Pt_2Sn_2 compounds.

	$E_g\,(Y \rightarrow X)$ (eV)				
$ScTaPd_2Sn_2$	GGA	LDA	EV-GGA	mBJ-GGA	mBJ-LDA
	0.416	0.447	0.549	0.425	0.453
ScTa Pt_2Sn_2	0.740	0.775	0.851	0.828	0.884

The EV-GGA approximation will be taken into account to describe other results in the parts that follow. We compare our DHH compounds results to those estimated earlier in Mekki *et al* [2]. because there are no other theoretical or empirical data to compare.

3.2. Electronic structure

We calculate the electronic characteristics of $ScTaPd_2Sn_2$ and $ScTaPt_2Sn_2$ at their equilibrium lattice parameters, along the high symmetry points in the first *Brillouin zone* of the simple orthorhombic structure $(\Gamma - X - S - Y - \Gamma - Z - U - R - T - Z - T - Y - S - R - U - X)$, by utilizing an assortment of exchange–correlation potentials, including EV-GGA and GGA. Figure 5 shows that $ScTaPd_2Sn_2$ and $ScTaPt_2Sn_2$ exhibit semiconductor behavior with an indirect band gap Y_v-X_c. The best values for this band gap are 0.549 eV and 0.851 eV, respectively, as determined by the EV-GGA approximation in table 4. The total density of states (DOS) and partial density of states (PDOS) plots for $ScTaPd_2Sn_2$ and $ScTaPt_2Sn_2$ exhibit significant similarities, as depicted in figure 6. it seems clear that the main contribution occupied by the Pd-d in the energy range of −5.475 eV to −2.128 eV also a few contributions of Ta-d states at the level of the valence band, the other side of the band structure which is the conduction band shows a slight contribution to the Pd -d whereas the Sc/Ta-d appear in strong contribution from the of the energy gap limit 0.542 eV to −6.035 eV. Initial analysis of the electronic properties indicates that our DHH and $ScNbNi2Sn_2$ demonstrate comparable characteristics.

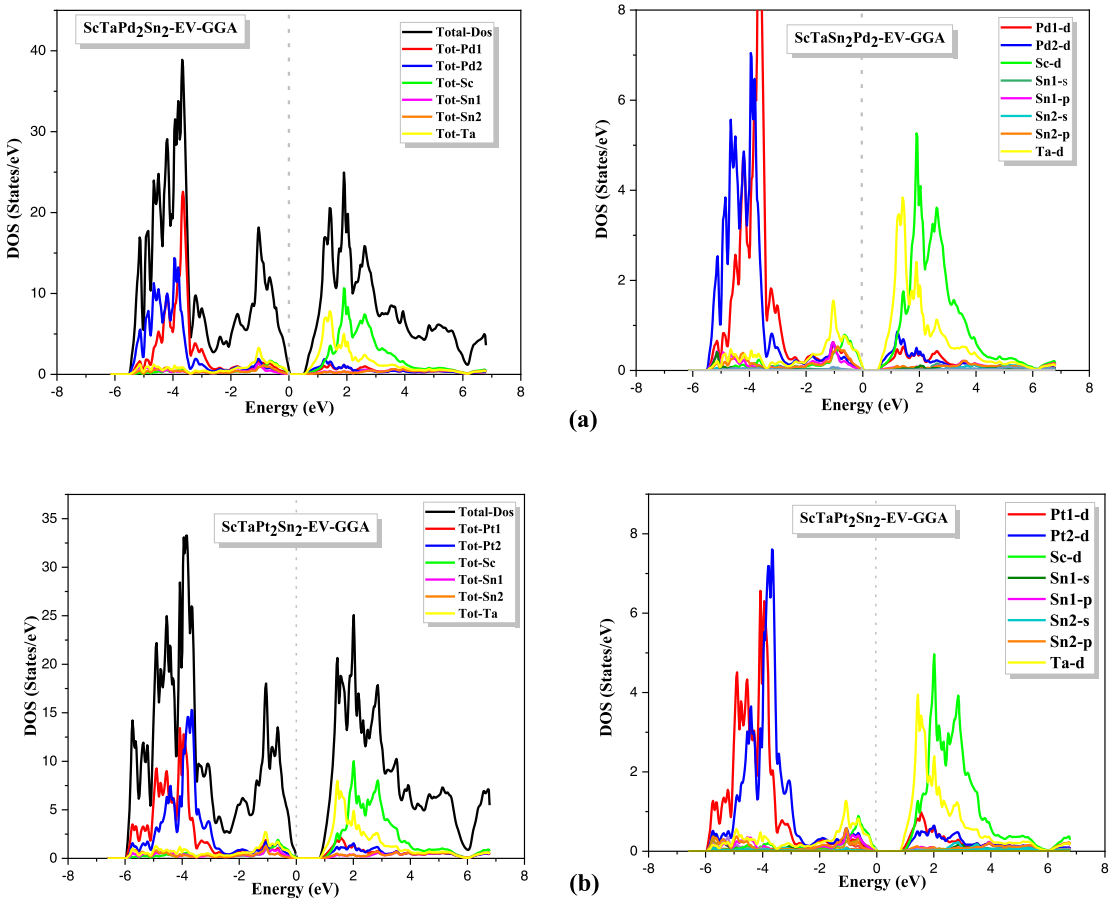

Figure 6. Orbital electronic density of sates for (a) $ScTaPd_2Sn_2$ and (b) $ScTaPt_2Sn_2$ using EV-GGA approximation.

3.3. Optical properties

The process by which that light interacts with the electrons in material defines its optical properties .as a result of providing a through description of the electronic structure and energy level of materials, DFT enables the prediction and analysis of the optical properties, so in this part of the results the optical properties has been calculated in the energy range from 0 up to 40 eV in the three directions x, y, and z-axes for $ScTaPd_2Sn_2$ and $ScTaPt_2Sn_2$ within EV-GGA. The complex dielectric constant describes the relationship between the incident wavelength of light and the optical properties of a material. It can be described as:

$$\varepsilon(\omega) = \varepsilon_1(\omega) + i\varepsilon_2(\omega) \tag{1}$$

Where $\varepsilon_2(\omega)$ represents the imaginary part, and on the other side $\varepsilon_1(\omega)$ represents the real part of the dielectric function can be obtained from the imaginary part Kramers-Kroning relation [22].

The dielectric functions' real $\varepsilon_1(\omega)$ and imaginary $\varepsilon_2(\omega)$ parts are plotted as a function of the energy of photons along the x, y, and z-axes in figures 7(a) and (b). The computed static values of $\varepsilon_1(0)$ for $ScTaPd_2Sn_2/ScTaPt_2Sn_2$ is found to be 15.764/13.687 for $\varepsilon_{1xx}(0)$, 15.635/13.652 for $\varepsilon_{1yy}(0)$ and 15.585/13.623 for $\varepsilon_{1zz}(0)$, respectively. The mean static value $\varepsilon_1(0)$ is 15. 661 for $ScTaPd_2Sn_2$ and 13.625 for $ScTaPt_2Sn_2$. Considering that there is a similarity between the two DHH compounds, we will pick $ScTaPd_2Sn_2$ for further investigation, as depicted in figure 7(a), the values start to rise from the $\varepsilon_1(0)$ and reach their peak at 33.372 for $\varepsilon_{1xx}(\omega)$, 36.261 for $\varepsilon_{1yy}(\omega)$ at 2.326 eV, and 31.636 for $\varepsilon_{1zz}(\omega)$ at 2.351 eV, respectively then They commence decreasing. The negative value of the real part indicates that $ScTaSn_2Pd_2$ can reflect incident photon radiations across a wide range of energy levels of 3.554 to 17.673 eV which corresponds to the semiconductor behavior. From figure 7(b) the imaginary part of the dielectric function $\varepsilon_2(\omega)$ reveal fundamental absorption threshold near 0.542 eV which represents the transition between the maximum valence band and the minimum conduction band .the highest peak value is 34.921 for $\varepsilon_{2xx}(\omega)$, 29.023 for $\varepsilon_{2yy}(\omega)$, and 26.873 for $\varepsilon_{2zz}(\omega)$ located at about 2.843 eV and 3.081eV respectively, that prove the anisotropy of $ScTaPd_2Sn_2$.

From figure 7(c) the high peaks of optical conductivity $\sigma(\omega)$ are located at 3.088 eV (14.511×10^3) for $\sigma_{xx}(\omega)$,3.931 eV for $\sigma_{yy}(\omega)$(12.759) and $\sigma_{zz}(\omega)$(11.981), for $ScTaPd_2Sn_2$. In the other hand the compound $ScTaPt_2Sn_2$ has the value of 16×10^3 at 3.523eV for $\sigma_{xx}(\omega)$,13.217 at 4.013 for $\sigma_{yy}(\omega)$ and 12.913 at 3.332 eV for

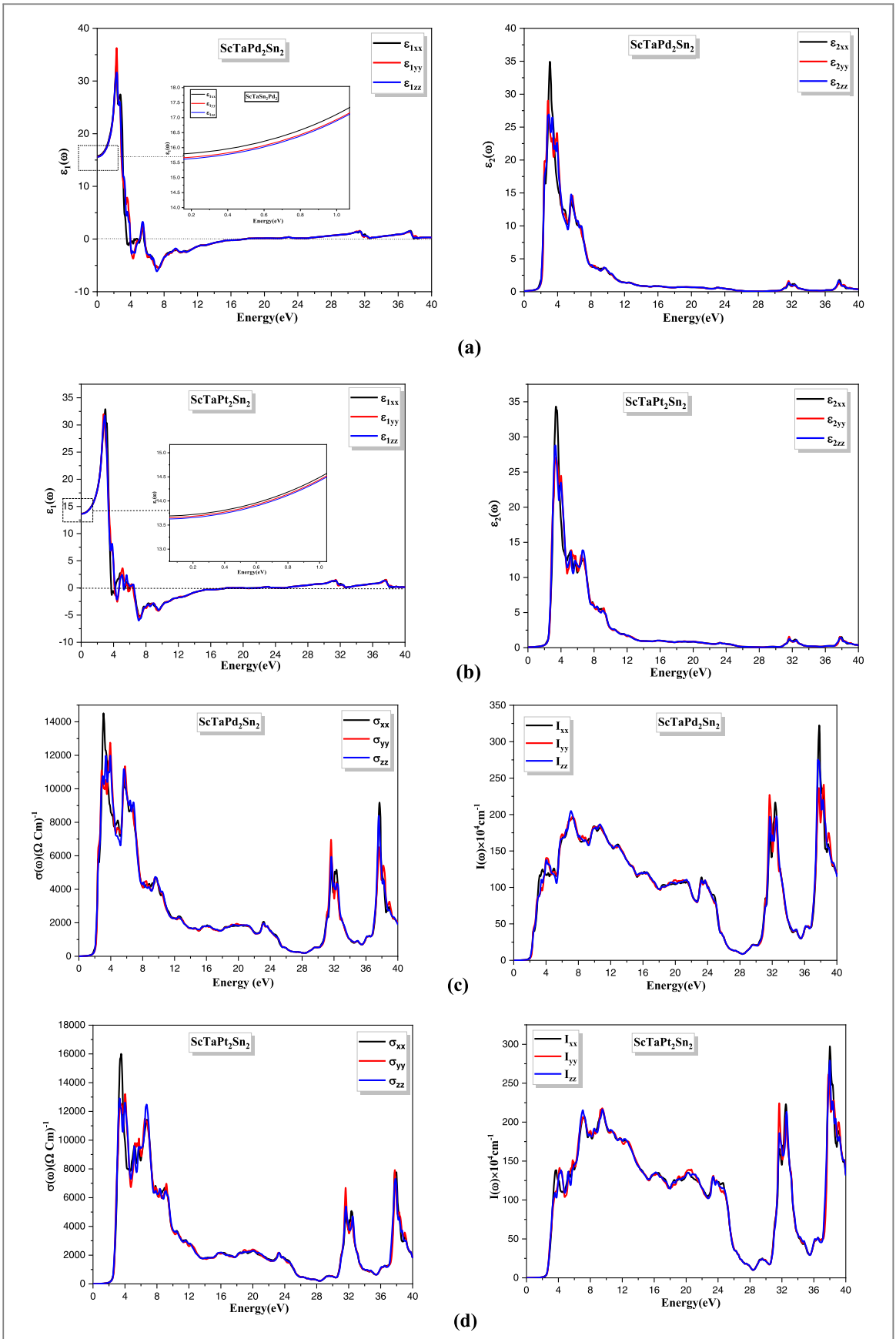

Figure 7. Variation of (a) the real, (b) the imaginary parts of the dielectric function, (c) optical conductivity, and (d) absorption coefficient for DHH $ScTaPd_2Sn_2$ and $ScTaPt_2Sn_2$ using EV-GGA approximation.

$\sigma_{zz}(\omega)$ respectively. The primary structure extends between the threshold and 28 eV .in addition, intermediate peaks appear up to 40 eV.

From figure 7(d) we can see that the absorption begins from the energy 1.52 eV/2 eV and increase gradually with the increasing of the photon energy then reaching a maximum value 204.9×10^4 cm^{-1} at 7.082 eV/217×10^4 cm^{-1} at 9.152 eV. Subsequently, the intensity rises once again, reaching an exceptionally high value of around 322 at 37.811 eV for $ScTaPd_2Sn_2$ and 297.421 at 38 eV for $ScTaPt_2Sn_2$, along the *x*-axis.

Figure 8(a) displays the extinction coefficient $k(\omega)$ which describe how strongly a DHH reflects the radiation, as we see in the curve the maximum values of $k_{xx}(\omega)$, $k_{yy}(\omega)$ and $k_{zz}(\omega)$ are 3.583, 3.451 and 3.365 at 3.193 eV, 4.014 eV and 4.042 eV for $ScTaPd_2Sn_2$ respectively while the compound $ScTaPt_2Sn_2$ has the values of 3.753, 3.376 and 3.192 at 3.635 eV, 4.121 eV and 4.104 eV . According to the figure 8(b) the refractive index begins at the following values 3.970 for $n_{xx}(0)$, 3.954 for $n_{yy}(0)$ and 3.9478 for $n_{zz}(0)$, respectively. The average quantity of $n(0)$ is precisely 3.9574, and it is directly related to $\varepsilon_1(\omega)$ by $n(0) = \sqrt{\varepsilon_1(0)} = \sqrt{15.6619} =$ 3.9574.The refractive index rise in the energy range 0–2.353 eV and reaches its maximum values 5.88,6.10 and 5.73 for n_{xx}, n_{yy}, and n_{zz} directions, respectively Thereafter, it gradually decreases as photon energy rises, this finding is equally evident in the $ScTaPt_2Sn_2$ compound see table 5.

The curve in the figure 8(c) represents the reflectance variation, the reflectance value is approximately 35.501% starting from the zero frequency, there are several intense peaks in the energy range 2.301–12.11 eV however the most intense has a reflectivity about 59.921%, while the $ScTaPt_2Sn_2$ compound has significantly same behavior as $ScTaPd_2Sn_2$.These compounds has a wide range of applications in the medical and space industries because it has a high reflectivity in the UV region. Figure 8(d) displays the change of the energy loss spectra function. The peaks observed in the spectra correspond to the plasma resonance, and the frequencies at which the resonant energy loss occurs are 17 eV for $ScTaPd_2Sn_2$, 15 eV for $ScTaPt_2Sn_2$, and 38 eV for all directions. The principal peak is located at 25 eV and 40 eV for $ScTaPd_2Sn_2$ and $ScTaPt_2Sn_2$ respectively.

3.4. Elastic properties

We use the IRelast package [23] implemented in Wien2k code to calculate the elasticity constants.in order to determine the compound's mechanical stability, nine independent elastic constants explain how an orthorhombic structure behaves elastically. These constants are: C_{11}, C_{22}, C_{33}, C_{12}, C_{13}, C_{23}, C_{44}, C_{55} and C_{66}., where C_{11}, C_{22} and C_{33} reflect the resistance to compression in one direction, respectively. however, the remaining ones show shear stress resistances (C_{12}, C_{13}, C_{23}, C_{44}, C_{55} and C_{66}). the GGA approximation was used to calculate the elastic properties. Table 6 show that C_{22} value of $ScTaPd_2Sn_2$ and $ScTaPt_2Sn_2$ is larger than C_{11} and C_{33} which indicate the strong resistance to deformation on the b-axis than the *c*-axis and the a-axis, therefore C_{11} and C_{22} are higher than those of Mekki *et al* [2] revealing that both compounds $ScTaPd_2Sn_2$ and $ScTaPt_2Sn_2$ has strong deformation resistance along a-axis and b-axis, also C_{44} has higher value comparing to $ScNbNi_2Sn_2$, as well as we can state that these DHH compounds display elastic anisotropy.

$$\begin{aligned} &C_{11} > 0, \quad C_{22} > 0, C_{33} > 0, \quad C_{44} > 0, C_{55} > 0, \quad C_{66} > 0, \quad [C_{11} + C_{22} - 2C_{12}] > 0, \\ &[C_{11} + C_{33} - 2C_{13}] > 0, [C_{22} + C_{33} - 2C_{23}] > 0, C_{11} + C_{22} + C_{33} + 2\ [C_{12} + C_{13} + C_{23}] > 0, \\ &\frac{1}{3}\ [C_{12} + C_{13} + C_{23}] < B < \frac{1}{3}\ [C_{11} + C_{22} + C_{33}] \end{aligned} \tag{2}$$

The calculated elastics constants satisfying the conditions of the stability criteria given in (11), accordingly, these materials are mechanically stable.

The Voigt-Reuss-Hill (VRH) approximation can be used to derive the bulk modulus (B) and shear modulus (G) of polycrystal materials from the obtained constants C_{ij} of a single crystal

And Hill's compressibility module and shear modulus are [24–26]:

$$G_H = \frac{1}{2}(G_V + G_R) \text{ and } B_H = \frac{1}{2}(B_V + B_R) \tag{3}$$

where B_V and G_V correspond to Voigt's bulk modulus and shear modulus, B_R and G_R are Reuss's bulk modulus and shear modulus, respectively, [27, 28].

The Young's modulus *E* and Poisson ratio σ [29] are calculated as follows

$$E = \frac{9BG}{(G + 3B)} \text{ and } \sigma = \frac{3B - 2G}{2(3B + G)} = \frac{1}{2}\left(1 - \frac{E}{3B}\right) \tag{4}$$

The bulk modulus reflects a material's resistance to volume change. The shear modulus reflects a material's resistance to shape change. The Young's modulus measures material stiffness, and the higher the value, the stiffer the material. Using the relations up above, all elastic modulus (compressibility modulus, *B*, shear modulus, *G*, Young modulus *E*, Poisson ratio σ and B/G ratio) for $ScTaSn_2Pd_2$, and $ScTaPt_2Sn_2$ have been calculated and presented in table 7. Start with the compressibility modulus B so $ScTaSn_2Pd_2$ has high value than

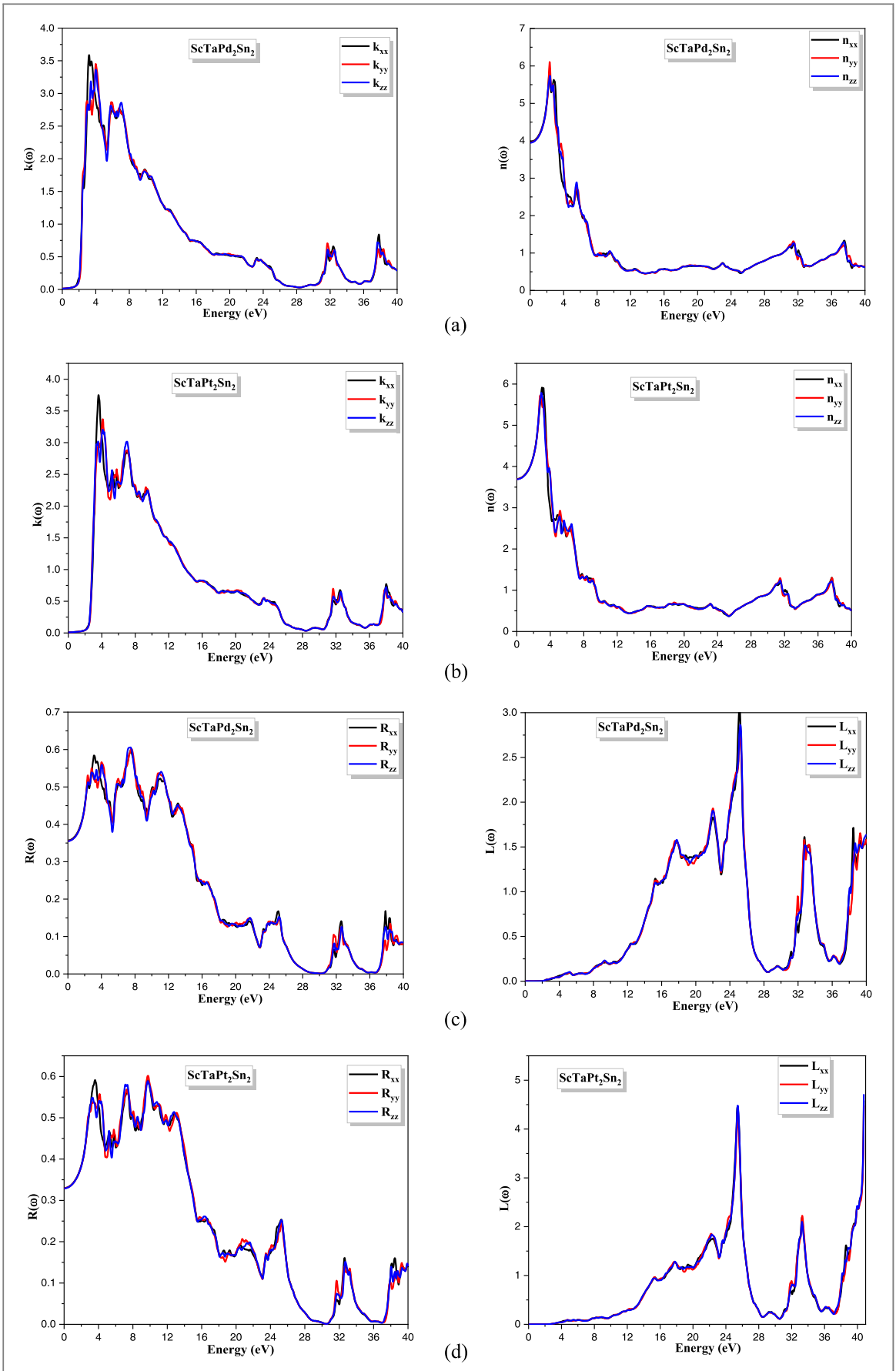

Figure 8. Variation of (a) the refractive index, (b) the extinction coefficient, (c) reflectivity spectra, and (d) the energy loss function as a function of photon energy for $ScTaPd_2Sn_2$ and $ScTaPt_2Sn_2$ within EV-GGA.

Table 5. Calculated static optical properties for $ScTaPd_2Sn_2$ compounds within different approximations.

$ScTaSn_2Pd_2$	$\varepsilon_1(0)$			$n(0)$			$R(0)$			$L(0)$		
Approximation	ε_{1xx}	ε_{1yy}	ε_{1zz}	n_{xx}	n_{yy}	n_{zz}	R_{xx}	R_{yy}	R_{zz}	L_{xx}	L_{yy}	L_{zz}
GGA	16.1305	15.9754	15.9316	4.0163	3.9969	3.9914	0.3615	0.3597	0.3591	3.9229×10^{-4}	3.9034×10^{-4}	3.9318×10^{-4}
EV GGA	15.7646	15.6355	15.5857	3.9704	3.9542	3.9478	0.3571	0.3555	0.3549	3.9927×10^{-4}	3.9832×10^{-4}	4.001×10^{-4}
mBJ GGA	15.8695	15.6844	15.6406	3.9836	3.9548	3.3954	0.3584	0.3561	0.3556	4.1623×10^{-4}	4.1519×10^{-4}	4.1865×10^{-4}
LDA	15.6574	15.4761	15.4339	3.9569	3.9339	3.9286	0.3558	0.3536	0.3530	4.0524×10^{-4}	4.0385×10^{-4}	4.0675×10^{-4}
mBJ LDA	15.4768	15.3006	15.2414	3.9340	3.91162	3.9040	0.3536	0.3514	0.3506	4.1406×10^{-4}	4.1332×10^{-4}	4.1623×10^{-4}

Table 6. Calculated static optical properties for $ScTaPt_2Sn_2$ compounds within different approximations.

$ScTaSn_2Pt_2$	$\varepsilon_1(0)$			$n(0)$			$R(0)$			$L(0)$		
Approximation	ε_{1xx}	ε_{1yy}	ε_{1zz}	n_{xx}	n_{yy}	n_{zz}	R_{xx}	R_{yy}	R_{zz}	L_{xx}	L_{yy}	L_{zz}
GGA	14.2820	14.2345	14.1907	3.7791	3.7728	3.7670	0.3381	0.3375	0.3369	3.797×10^{-4}	3.778×10^{-4}	3.797×10^{-4}
EV GGA	13.687	13.652	13.623	3.6434	3.6388	3.6347	0.3240	0.3236	0.3231	4.104×10^{-4}	4.086×10^{-4}	4.105×10^{-4}
mBJ GGA	13.179	13.162	13.110	3.633	3.627	3.620	0.3227	0.3224	0.3216	4.105×10^{-4}	4.08×10^{-4}	4.109×10^{-4}
LDA	13.8641	13.8333	13.7784	3.7234	3.7193	3.7119	0.3324	0.3320	0.3312	3.957×10^{-4}	3.935×10^{-4}	3.959×10^{-4}
mBJ LDA	13.2354	13.1903	13.1555	3.6386	3.6318	3.6270	0.3235	0.3228	0.3223	4.098×10^{-4}	4.086×10^{-4}	4.105×10^{-4}

Table 7. The computed elastic constants for $ScTaSn_2Pd_2$, and $ScTaSn_2Pt_2$ using GGA.

Elastic constants (GPa)	$ScTaPd_2Sn_2$	$ScTaPt_2Sn_2$
C_{11}	244.5670	275.1153
C_{22}	246.9794	277.4895
C_{33}	198.7872	226.3281
C_{44}	97.0080	108.2926
C_{55}	94.0026	104.3802
C_{66}	47.3981	54.3908
C_{12}	57.8910	66.4894
C_{13}	104.2453	115.6720
C_{23}	106.8555	120.1886
A_1	1.6521	1.6037
A_2	1.6203	1.5848
A_3	0.5045	0.6772

Table 8. Modules of elasticity B_V, B_R, B_H, G_V, G_R, G_H,E_V,E_R, E_H, σ_V, σ_R, σ_H for $ScTaPd_2Sn_2$ and $ScTaPt_2Sn_2$ using *GGA* approximation.

Elasticity modules (GPa)	$ScTaPd_2Sn_2$	$ScTaPt_2Sn_2$
B_V	136.479	153.736
B_R	136.472	153.722
B_H	136.475	153.729
G_V	75.77	85.184
G_R	67.391	76.602
G_H	71.58	80.893
E_V	191.813	215.710
E_R	173.598	197.071
E_H	182.783	206.464
σ_V	0.265	0.266
σ_R	0.287	0.286
σ_H	0.276	0.276
B_H/G_H	1.906	1.9003
A_B%	2.56×10^{-3}	4.55×10^{-3}
A_G%	5.852	5.3045
A^u	0.621	0.5602

the $ScNbNi_2Sn_2$ compound ($B_{H\ ScTaPt2Sn2} = 153.72$ GPa $> B_{H\ ScTaPd2Sn2} = 136.47$ GPa) which indicate that $ScTaPt_2Sn_2$ exhibit elastic stiffness more than the $ScTaPd_2Sn_2$, as well as, The zero-pressure bulk modulus reported in table 8 is close to that from the equation of Murnaghan (EOS) for the $ScTaPd_2Sn_2$ and $ScTaPt_2Sn_2$ compounds. These compounds have a high shear modulus (71.5 GPa, and 80.8 GPa) it can be notice that $ScTaPt_2Sn_2$ display large shear modulus than $ScTaPd_2Sn_2$.

Pugh [30] introduced the bulk to shear modulus (B/G) ratio as an indicator of ductile versus brittle characteristics. If the B/G ratio is more than 1.75, the material is ductile, otherwise, the material is brittle. Both compounds have B/G ratios greater than 1.75, indicating that DHH compounds are ductile. The ratio of tensile stress to tensile strain is defined as the young modulus E which is large for $ScTaPt_2Sn_2$ compared to the compound $ScTaPd_2Sn_2$.

The dimensionless amount the Poisson's ratio is a measure of how well a material resists lateral deformation. For stable compounds, the Poisson's ratio value of a solid is −1 to 0.5 [31]. Table 8 shows the Poisson's ratio value is about 0.276 for the DHH which confirms that these compounds are stable under shear stress, this suggests that $ScTaPd_2Sn_2$ and $ScTaPt_2Sn_2$ are contracted by 27.6%.

The Debye temperature θ_D is the temperature of a crystal's highest normal mode of vibration, and it correlates the elastic properties with the thermodynamic properties such as phonons, thermal expansion, thermal conductivity, specific heat, and lattice enthalpy [32]. The Debye temperature [33] can be calculated using the average sound velocity, the temperature of Debye θ_D can be determined as follows [33, 34].

The computed sound velocity and Debye temperature for DHH compounds are displayed in table 9. All DHH compounds seem to have computed Debye temperatures above 300 K implying that they share the same Debye temperature and melting point.

Table 9. Acoustic sound velocities (V_l,V_t, V_m in m/s), and Debye temperature (θ_D in K) for $ScTaPd_2Sn_2$, and $ScTaPt_2Sn_2$ DHH alloys using *GGA* approximation.

Compounds	V_t (m/s)	V_l (m/s)	V_m (m/s)	θ_D(K)
$ScTaPd_2Sn_2$	2783.84	5010.86	3100.51	338.605
$ScTaPt_2Sn_2$	2652.3	4769.52	2953.78	321.105

Zener anisotropy A is an indicator for the degree of anisotropy in the bonding between atoms in various planes and quantified by the shear anisotropic factors. for the shear anisotropy factor for the {100} shear planes between the ⟨011⟩ and ⟨010⟩ directions is [35]

$$A_1 = 4C_{44}/(C_{11} + C_{33} - 2C_{13}) \tag{5}$$

For the shear anisotropy factor for the {010} shear planes between the ⟨101⟩ and ⟨001⟩ directions [35]

$$A_2 = 2C_{66}/(C_{11} - C_{12}) \tag{6}$$

Finally, for the shear anisotropy factor for the {001} shear planes between the ⟨110⟩ and ⟨010⟩ directions is [35]

$$A_3 = 4C_{66}/(C_{11} - 2C_{12} + C_{22}) \tag{7}$$

As well, for isotropic crystals, the factors A_1, A_2 and A_3 must be one. We might confirm that the crystal has elastic anisotropy if any of the three factors is lower or larger than one the crystal represents the degree of the anisotropy.

From table 7 it seems that the shear anisotropy of $ScTaPd_2Sn_2$ and $ScTaPt_2Sn_2$ is larger for (100) and (010) shear planes

The percentage anisotropy for the bulk modulus A_B and shear modulus A_G is given by [36]

$$\begin{cases} A_B = (B_V - B_R)/(B_V + B_R) \times 100 \\ A_G = (G_V - G_R)/(G_V + G_R) \times 100 \end{cases} \tag{8}$$

The universal anisotropy index (A^U) is given by [37]:

$$A^U = 5\frac{G_V}{G_R} + \frac{B_V}{B_R} - 6 \tag{9}$$

The values of A_B, A_G, and A^U must be zero for an isotropic material. The degree of anisotropy is represented by a deviation larger than zero. From table 8 the percentage of bulk modulus A_B% for $ScTaPd_2Sn_2$, and $ScTaPt_2Sn_2$ is zero because the Voigt and Reuss approaches anticipate the same values for the bulk modulus, indicating that these compounds are slightly isotropic in compressibility. Likewise, the value of the shear modulus percentage for $ScTaSn_2Pd_2$ and $ScTaPt_2Sn_2$ are 5.8% 5.3% shear modulus respectively. Thus, are characterized by significant anisotropy in shear modulus and isotropy in bulk modulus.

The study mentioned above is insufficient to adequately characterize the elastic properties of a crystal. Surface structures that show the linear compressibility and the reciprocal of Young's modulus with directions are useful in fact. The orthorhombic system's linear compressibility is [38]:

$$\beta = n_1^2(S_{11} + S_{12} + S_{13}) + n_2^2(S_{12} + S_{22} + S_{23}) + n_3^2(S_{13} + S_{23} + S_{33}) \tag{10}$$

S_{ij} are the elastic constants of deformability, and n_1, n_2, n_3: are the directional cosines (in spherical coordinates) following *x*, *y* and *z*, respectively.

The orthorhombic system defines the reciprocal of Young's modulus E in the direction of the unit vector n_i as [38]:

$$E = \frac{1}{n_1^4 S_{11} + 2n_1^2 n_2^2 S_{12} + 2n_1^2 n_3^2 S_{13} + n_2^4 S_{22} + 2n_2^2 n_3^2 S_{23} + n_3^4 S_{33} + n_2^2 n_3^2 S_{44} + n_1^2 n_3^2 S_{55} + n_1^2 n_2^2 S_{66}} \tag{11}$$

The linear compressibility of $ScNbPd_2Sn_2$, and $ScNbPt_2Sn_2$ is determined using the theoretical elastic constants depicted in figure 9. The equation (10) establish a three-dimensional surface, where the distance from the origin of coordinates to the surface corresponds to the linear compressibility in a certain direction. The cubic system exhibits isotropic linear compressibility, resulting in a spherical form. The spherical form of figure 9 illustrates the isotropic nature of linear compressibility of our two alloys $ScTaPd_2Sn_2$, and $ScTaPt_2Sn_2$. To obtain a more detailed and full understanding of the anisotropic features, it is necessary to examine the orientation-dependent linear compressibility in different planes. The elastic anisotropy in the (XY) plane is slightly higher than in the (XZ) plane for $ScTaPd_2Sn_2$ alloy. Additionally, the (YZ) plane has the highest elastic anisotropy. However, in the $ScTaPt_2Sn_2$ alloy, the (XZ) plane has a larger elastic anisotropy than both the (XY) and (YZ) planes. Figure10

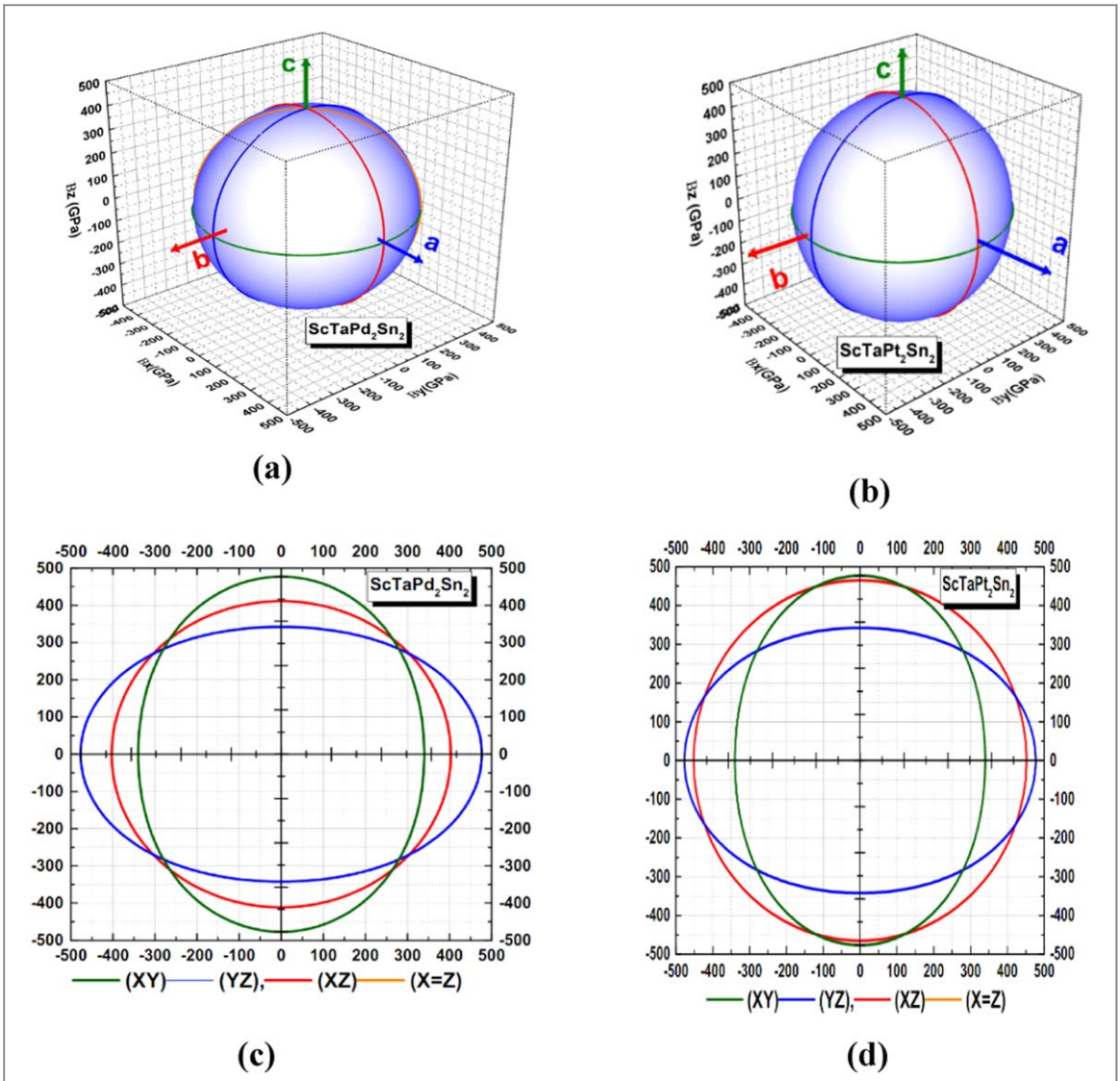

Figure 9. (a) and (b) represent the orientation dependent linear compressibility of, $ScTaPd_2Sn_2$ and $ScTaPt_2Sn_2$ respectively . (c) and (d) represent linear compressibility projections in different planes of $ScTaPt_2Sn_2$ and $ScTaPd_2Sn_2$ respectively.

depicts the predicted orientation-dependent Young's modulus for $ScTaPd_2Sn_2$, and $ScTaPt_2Sn_2$ alloys by employing the elastic compliance constants. A three-dimensional closed surface is defined by equation (11) when the distance between the surface and the origin of coordinates is equal to Young's modulus in the specified direction. Evidently, the surfaces representing Young's modulus for both alloys $ScTaPd_2Sn_2$, and $ScTaPt_2Sn_2$ exhibited non-spherical shapes Consequently, these two compounds have a significant degree of anisotropy because of the different bonding characteristics between adjacent atomic planes.

The alloys $ScTaPd_2Sn_2$ and $ScTaPt_2Sn_2$ display a large elastic anisotropy in the (XY) plane while (X = Y), (XZ) and (YZ) planes are almost identical.

3.5. Thermoelectric properties

3.5.1. Lattice thermal conductivity

Weak lattice thermal conductivity is a necessary characteristic for possible thermoelectric materials. We investigated the electronic transport properties of $ScTaPd_2Sn_2$ and $ScTaPt_2Sn_2$ DHH, such as the Seebeck coefficient S, electrical conductivity σ/τ, the figure of merit ZT and the thermal conductivity ($\kappa_{Tot} = \kappa_e + \kappa_L$) which is equal to the sum of the electronic thermal conductivity κ_e and the lattice thermal conductivity κ_L. The slacks formula is a widely used method for estimating κ_L [39, 40].

The lattice thermal conductivity k_L was determined using Slack's equation and the BoltzTraP code was used to assess the electronic thermal conductivity k_e. The Debye temperature has been determined using a quasi-harmonic Debye model that was included in the original Gibbs code [41–44].

Constant relaxation time estimation was utilized in our calculation $\tau = 3 \times 10^{-14}$ s for temperatures ranging from 50 K to 1000 K [45]. .the lattice thermal conductivity K_L represented in figure 11(a) which reveals a

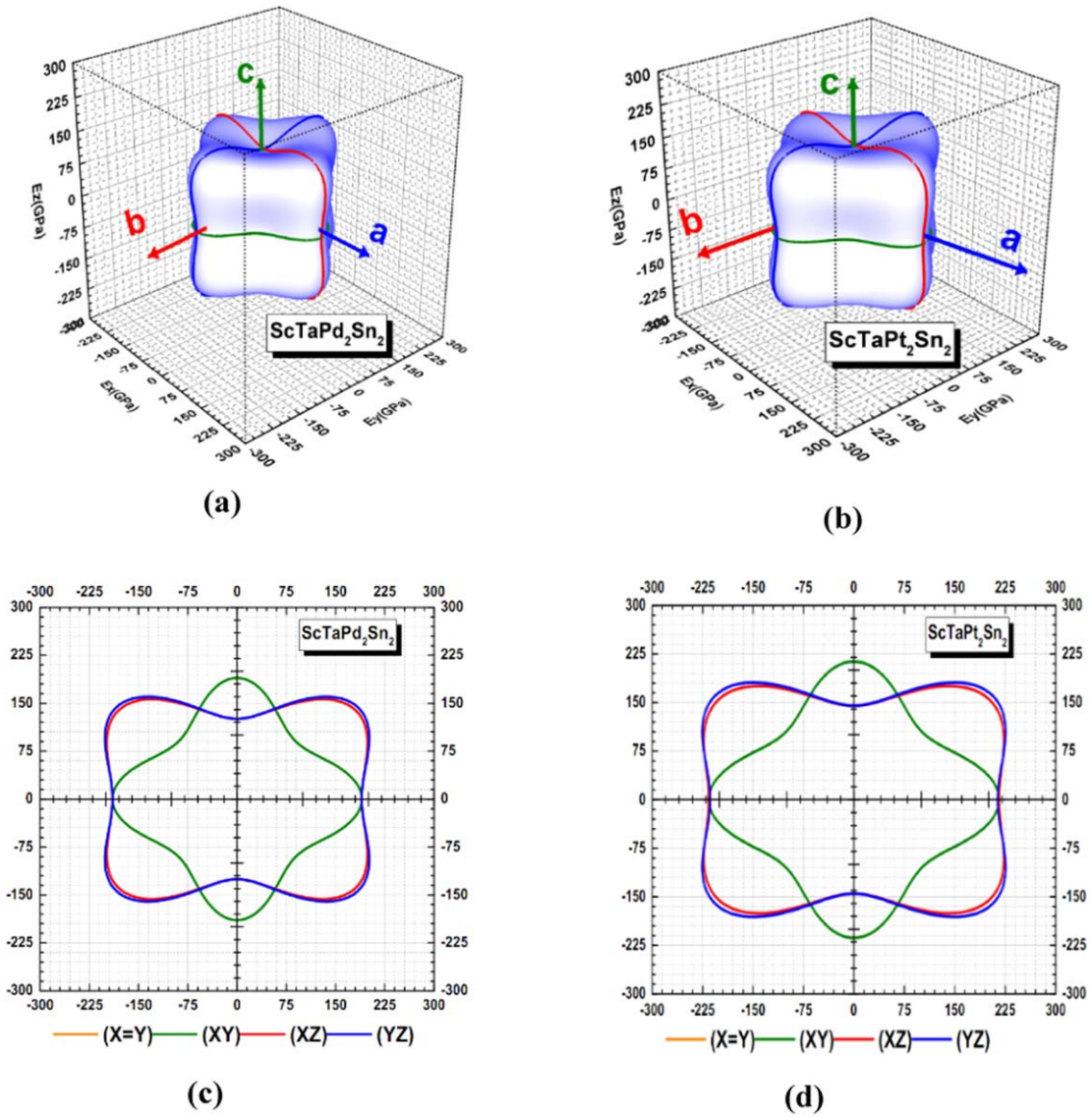

Figure 10. (a) and (b) represent the 3D surface of the Young's modulus for, $ScTaPd_2Sn_2$ and $ScTaPt_2Sn_2$, (c) and (d) their cross sections in different planes respectively.

significant reduction in the low temperature range <300 K, then progressively lowers against temperature due to the phonon interaction in the lattice. On the other hand, at room temperature the magnitude of K_L is 4.97 W K^{-1}.m for $ScTaPd_2Sn_2$ and 4.98 W K^{-1}.m for $ScTaPt_2Sn_2$ which are relatively larger value comparing to the existing DHH $ScNbNi_2Sn_2$ (5.3 W K^{-1}.m). Thus, low thermal conductivity is desirable in thermoelectric energy conversion materials. The electronic thermal conductivity K_{el} can be mathematically defined by the Wiedemann–Franz law, which asserts that the ratio of a metal's electronic thermal conductivity to electrical conductivity σ is proportional to temperature T.

($k_e/\sigma = LT$), where L stands for the Lorentz number. The electronic thermal conductivity of our material is shown in figure 11(b), As the temperature rises, there is definitely a linear increase due to the excitation of the electrons. As previously stated, thermal conductivity is the sum of electronic and lattice thermal conductivity, and K_T displayed in figure 11(c) appears to have the same behavior as K_L.

3.5.2. Transport properties

The relaxation time approximation can be used to calculate the transport coefficients (σ, S, and k_e) of the $ScTaSn_2Pd_2$ compound [46–49].

The electronic thermal conductivity components can also be derived using the Wiedemann–Franz law [50], $K_e = LT\sigma$, L is the Lorentz number

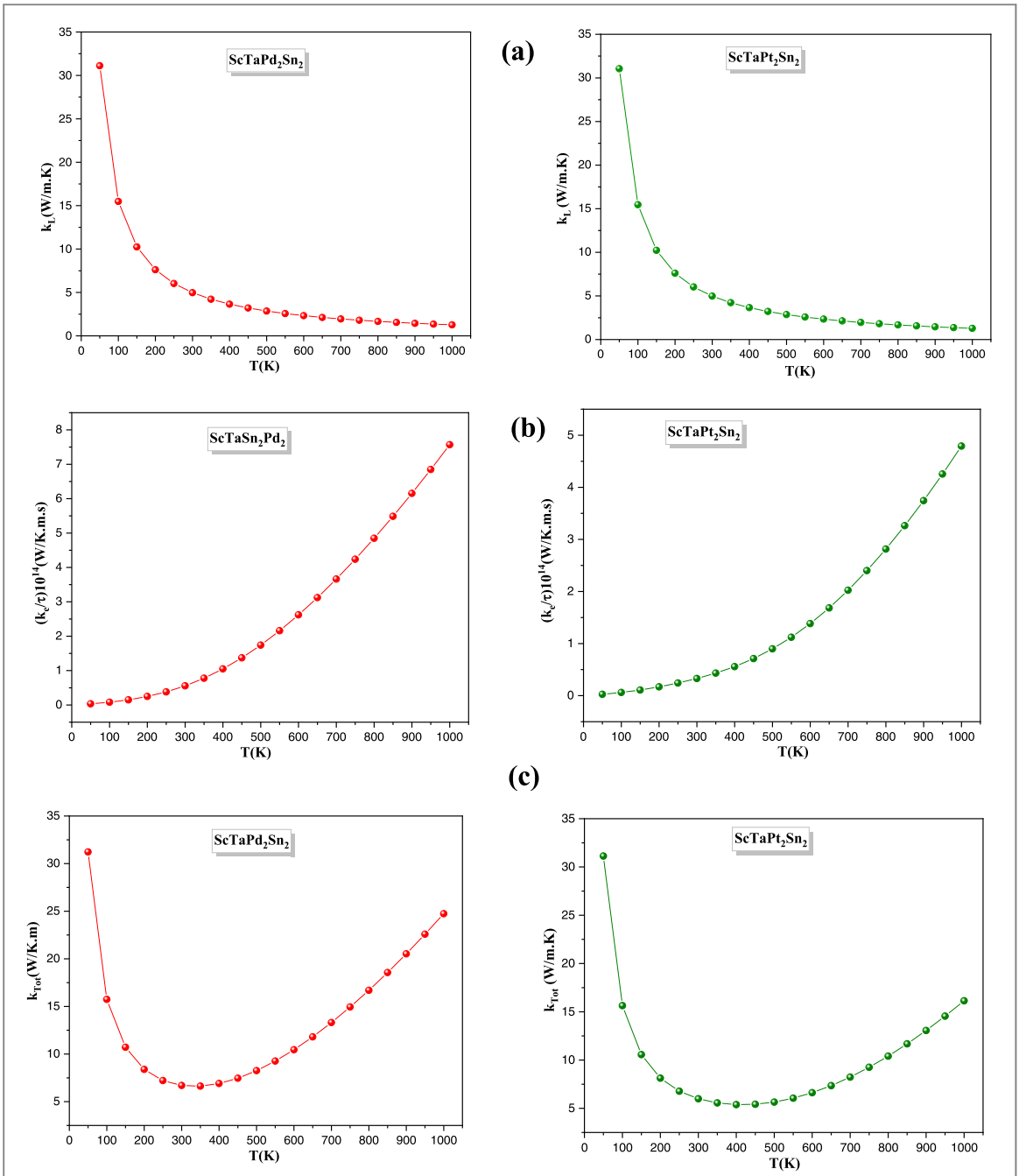

Figure 11. Temperature dependency of (a) lattice the thermal conductivity, (b)electronic thermal conductivity, (c) the total thermal conductivity of $ScTaPd_2Sn_2$ and $ScTaPt_2Sn_2$ compounds.

Figure 12(a) depicts the electrical conductivity σ/τ of the DHH compounds $ScTaPd_2Sn_2$ and $ScTaPt_2Sn_2$ as a function of temperature. We can clearly see the increase in electronic conductivity as the temperature rises, at room temperature, it has the value of 3.91×10^{18} $(\Omega.m.S)^{-1}$ and 2.79×10^{18} $(\Omega.m.S)^{-1}$ respectively.

The Seebeck coefficient is a measurement of the voltage produced across a material when a temperature gradient is applied to it, and it is defined as: $S = V/\Delta T$, Thus the figure 12(b) shows the Seebeck coefficient as a function of temperature hence, at room temperature ($T = 300$ K) $S_{ScTaPd2Sn2} = 173.8$ $\mu V/K$, $S_{ScTaPt2Sn2}$=138.7 $\mu V/K$ and reached a maximum value $S_{ScTaPd2Sn2} = 211.2$ $\mu V/K$, $S_{ScTaPt2Sn2} = 246.35$ $\mu V/K$ at $T = 750$ K and $T = 950$ K These values are much lower than the previous DHH $ScNbNi_2Sn_2$ findings ($S = 173.2$ $\mu V/K$ at 300 K, $Smax = 226.8$ $\mu V/K$ at 650 K). So both DHHs materials exhibit a positive Seebeck value across the temperature range, indicating that holes or positive charge carriers are the dominating charge carriers, confirming that our materials are p-type. The band structure degeneracy plays a crucial role in determining the thermoelectric properties of materials such as $ScTaPd_2Sn_2$ and $ScTaPt_2Sn_2$. The presence of multiple energy valleys along the k-path leads to enhanced Seebeck coefficients due to the increased density of states contributing to charge carrier transport. This phenomenon arises from the overlap of electronic bands, resulting in a higher effective mass for

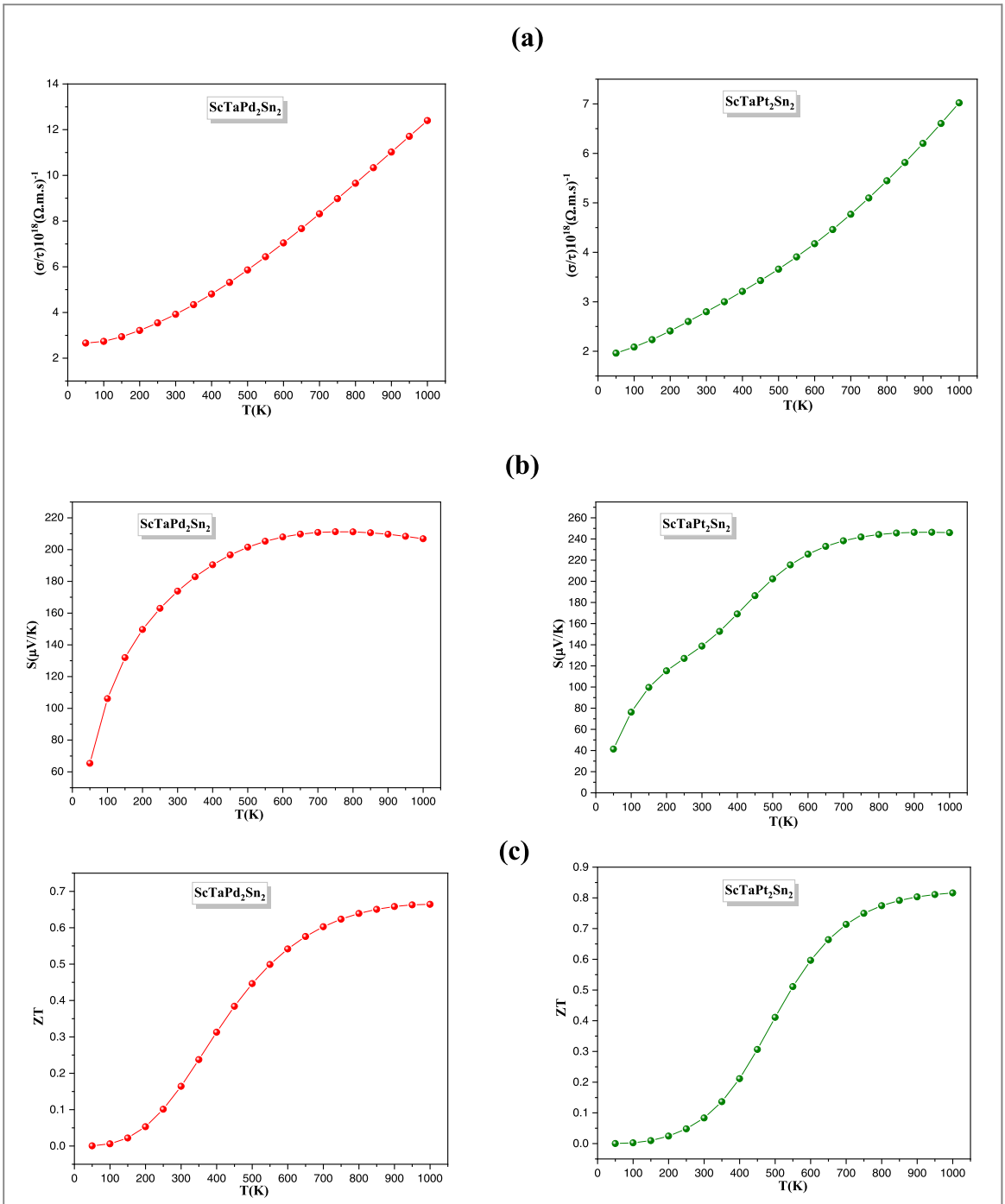

Figure 12. (a) The electrical conductivity per relaxation time (b) the coefficient of Seebeck, (c) the figure of merit ZT of $ScTaPd_2Sn_2$ and $ScTaPt_2Sn_2$ compounds.

charge carriers and consequently, a higher Seebeck coefficient. Additionally, the degeneracy of bands can facilitate improved carrier mobility, reducing scattering events and enhancing thermoelectric performance. Understanding and manipulating the band structure degeneracy through techniques such as alloying, doping, and strain engineering offer promising avenues for further enhancing the thermoelectric efficiency of these materials.

The figure of merit (ZT) is a significant measure used to assess a material's thermoelectric efficiency for energy conversion applications. Figure 12(c) illustrates the way ZT increases with temperature. at 900 K ZT are 0.664 and 0.816 for $ScTaPd_2Sn_2$ and $ScTaPt_2Sn_2$ respectively within EV-GGA. Researchers have recently been working on a new DHHs compounds due to its performance in thermoelectric applications. Figure 13 shows thermoelectric figure of merit ZT as a function of the temperature for DHH compounds $ScTaPd_2Sn_2$ and $ScTaPt_2Sn_2$ as well as $ScNbNi_2Sn_2$ [2] and $TiZrCo_2Bi_2$, $TiHfCo_2Bi_2$ and $ZrHfCo_2Bi_2$ [5]. We can observe that ZT increases with temperature for all DHH compounds, at 300 K the ZT values are 0.79, 0.76 and 0.8 for $TiZrCo_2Bi_2$

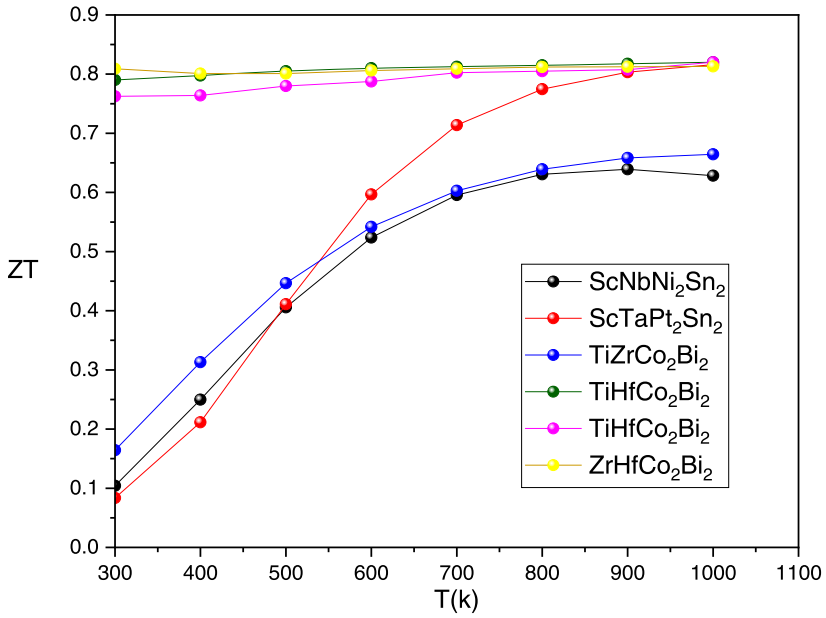

Figure 13. Thermoelectric figure of merit ZT of DHH compounds $ScTaPd_2Sn_2$ and $ScTaPt_2Sn_2$. Data are taken from ref $ScNbNi_2Sn_2$ [2] $TiZrCo_2Bi_2$, $TiHfCo_2Bi_2$, $TiZrCo_2Bi_2$ [5].

Table 10. The calculated of electrical conductivity tensor, the Seebeck coefficient tensor, and the electronic thermal conductivity of the DHH alloys $ScTaPd_2Sn_2$, and $ScTaPt_2Sn_2$ at 300 K and 1000 K within EV-GGA.

Alloys	T (K)	$\sigma/\tau^{*}10^{18}$ (W.m.s)$^{-1}$			S (μV/K)			ke/$\tau^{*}10^{14}$ (W/m.K)		
$ScTaPd_2Sn_2$	**1000**	16.59	6.43	14.15	208.99	197.63	213.83	10.47	3.46	8.76
	300	6.11	1.80	3.83	152.08	198.03	171.36	0.76	0.31	0.58
$ScTaPt_2Sn_2$	**1000**	12.35	1.48	7.22	197.97	305.35	234.65	7.32	1.64	5.4
	300	5.78	0.18	2.42	116.78	149.55	149.55	0.67	0.02	0.28

$TiHfCo_2Bi_2$ and $ZrHfCo_2Bi_2$ DHH compounds respectively all the three compound are p-type, likewise the ZT of the parent about 1.42 at 973 K [5], obviously all DHH are suitable for higher temperatures. Further, ZT = 0.99 and ZT = O.74 at 300 K for TiPtSb HH compound in spin dn and spin up channel respectively with P-type, also 0.95,0.97 and 0.98 for TiRuSb-dn, TiRuSb-up and $Ti_2RuPtSb_2$ with n-type [6], PtHfSn 0.57 and PtZrSn 0.24 in the p-type region [51].

Similarly, we compute the Seebeck coefficient, electrical conductivity and electronic thermal conductivity along the x,y and z axes, considering that Tensors ($\sigma_{xx} \neq \sigma_{yy} \neq \sigma_{zz}$), ($S_{xx} \neq S_{yy} \neq S_{zz}$), ($k_{e_{xx}} \neq k_{e_{yy}} \neq k_{e_{zz}}$) are diagonal.

Figure 14(a) display the Seebeck coefficient of $ScTaPd_2Sn_2$ compound in the three direction x,y and z,it appears that S_{xx} and S_{yy} stratify slightly at 50 K with the values 46.24 μV/K and 55.7 μV/K then increase linearly with temperature, reaching a maximum value at 750 K for S_{zz}, However S_{zz} (222.4 μV/K) has a greater value than S_{xx} (208.9 μV/K) and S_{YY} (212 μV/K). The largest value among all tensors has been found to be along the yy axes, as indicated by the highest value of S_{yy} for temperatures of 1000 K and 300 K, as given in table 10. This suggests that the yy-axis is the dominant factor in transport. In the other hand, figure 15(a) depicts the Seebeck coefficient of $ScTaPt_2Sn_2$ compound in the three direction x,y and z, it appears that S_{xx} and S_{zz} stratify slightly at 50 K with the values 49.58 μV/K and 49.85 μV/K then increase linearly with temperature, reaching a maximum value for all directions at 1000 K, However S_{yy} (305 μV/K) has a greater value than S_{xx} (197.9 μV/K) and S_{zz} (234.6 μV/K).

3.5.3. Strategies for improving the seebeck coefficient

Figure 16 displays a variation in the Seebeck coefficient within the temperature range of 300–800 K and 300–900 K for $ScTaPd_2Sn_2$ and $ScTaPt_2Sn_2$, respectively. The value of Seebeck coefficient for the alloys $ScTaPd_2Sn_2$ and $ScTaPt_2Sn_2$ are S = 211.15 μV/K at T = 800 K and S = 246.26 μV/K at T = 900 K which correspond to a carrier concentration of n = 4. 92 $\times$ 10^{20} Cm^{-3} at and n = 3. 34 $\times$ 10^{20} Cm^{-3} respectively. In order to enhance the thermoelectric properties of double half Heusler alloys, we conducted a study on the effects

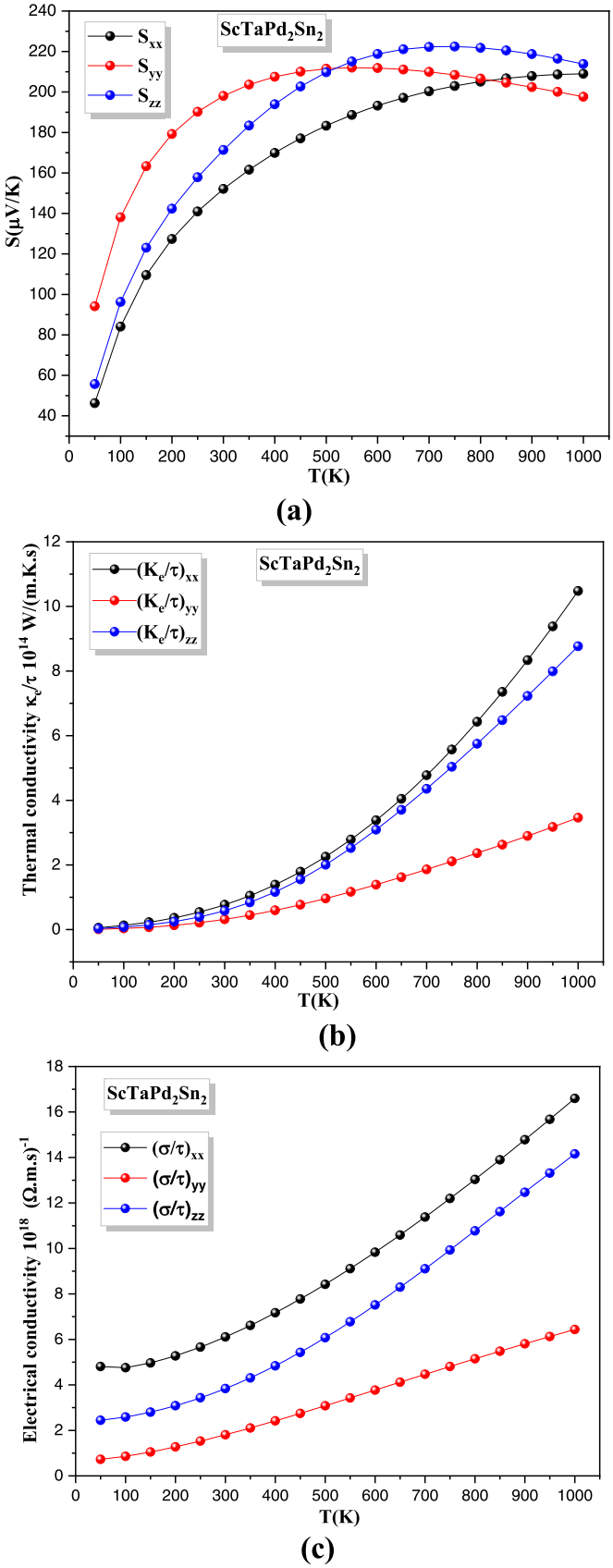

Figure 14. Computed the anisotropic transport characteristics of $ScTaPd_2Sn_2$ compound (a) Seebeck coefficient (b) electronic thermal conductivity and (c) ratio of electrical conductivity tensors component.

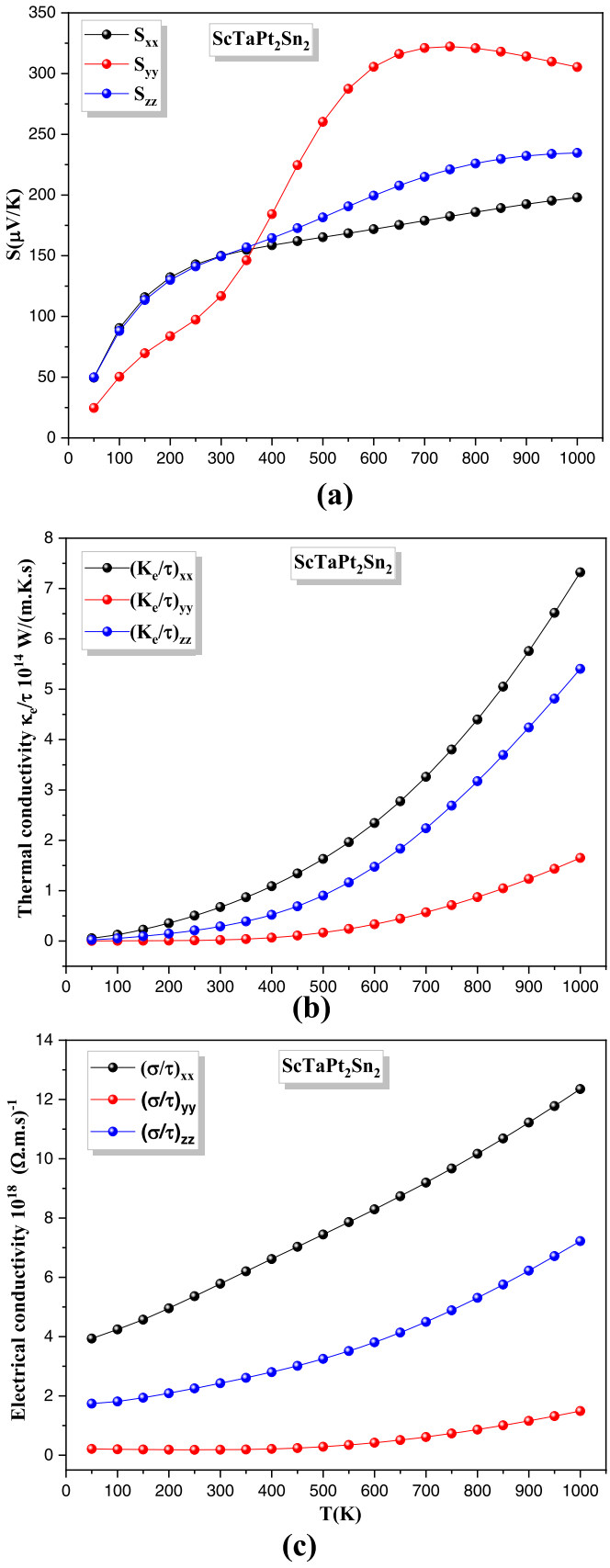

Figure 15. Computed the anisotropic transport characteristics of $ScTaPt_2Sn_2$ compound (a) Seebeck coefficient (b) electronic thermal conductivity and (c) ratio of electrical conductivity tensors components.

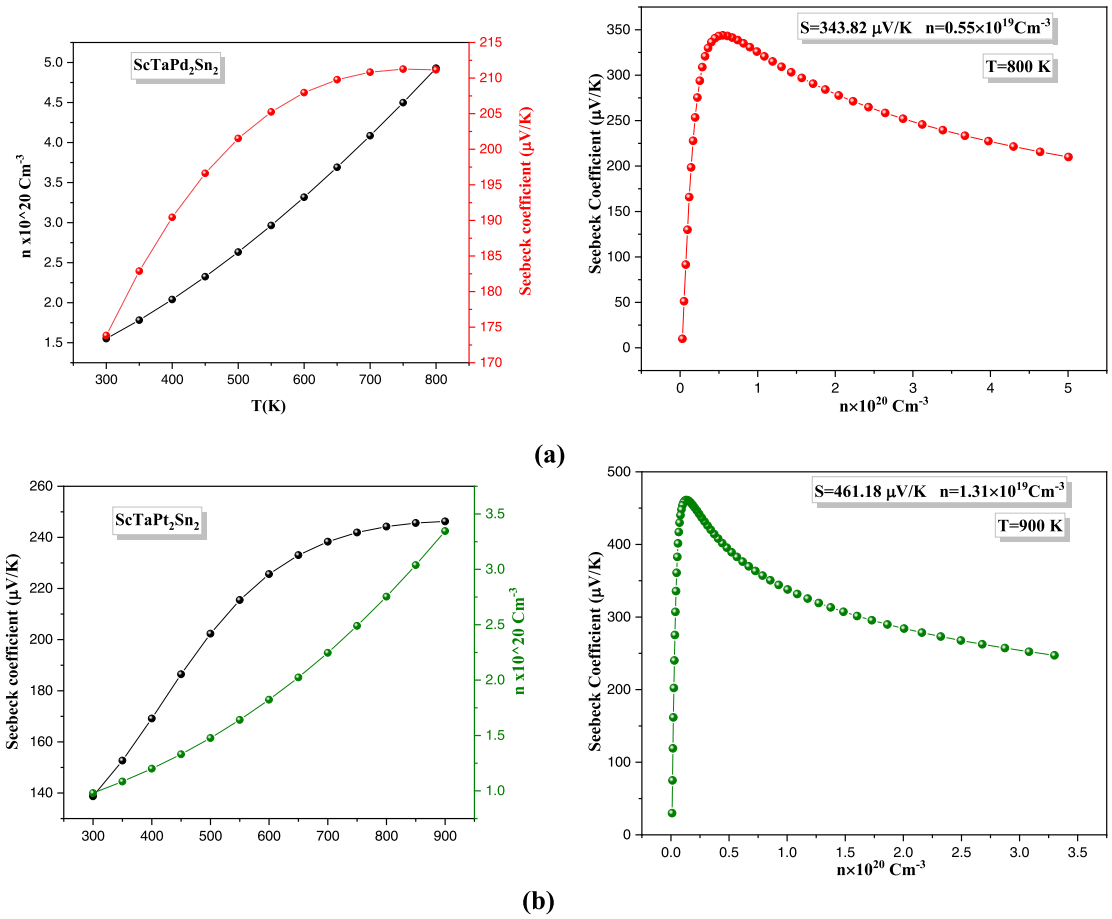

Figure 16. The figure of merit ZT of the DHH alloys (a) $ScTaPd_2Sn_2$ and (b) $ScTaPt_2Sn_2$ as a function of the concentration in charge carriers at fixed temperature (T = 800,900 K).

of carrier concentration on the Seebeck coefficient at a temperature of 800 K and 700 K for $ScTaPd_2Sn_2$ and $ScTaPt_2Sn_2$, respectively. Based on the data provided in figure 15 it is evident that the maximum values of Seebeck coefficient are 343.82 μV/K and 461.18 μV/K, these values occur when the concentration of charge carriers is reduced to a point where $n = 0.55 \times 10^{19}\ Cm^{-3}$ and $n = 1.31 \times 10^{19}\ Cm^{-3}$, $ScTaPd_2Sn_2$ and $ScTaPt_2Sn_2$, respectively.

3.5.4. Methods for enhancing the merit figure ZT

Based on figure 17, the lattice thermal conductivity values for all the DHH alloys $ScTaPd_2Sn_2$ and $ScTaPt_2Sn_2$ are low as a result of the described disorder. As the temperature rises, the values of k_L decrease and are almost equal to zero at extremely high temperatures. In this situation, we can determine an estimated value of without the need to calculate the average value of:

$$ZT \sim T\frac{S^2(\sigma/\tau)}{(k_e/\tau)} = T\frac{S^2\sigma}{k_e} \tag{12}$$

The rigid band approximation (RBA) assumes that the band structure of a system remains unchanged whether the temperature or doping is altered [52]. We investigated the relation between the figure of merit and the carrier concentration at a temperature of T = 900 K for double half Heusler, respectively. Figure 16 indicates that the $ScTaPd_2Sn_2$ alloy has a maximum ZT value 0.74, which is achieved by the n-doped material (n-type semiconductor) with an optimal carrier concentration of $-2 \times 10^{20}\ Cm^{-3}$ whereas for a p-type semiconductor, the highest ZT value is around 0.76 with carrier concentration $n = 2.66 \times 10^{20}\ Cm^{-3}$. Regrading to $ScTaPt_2Sn_2$ alloy which has the best enhancing figure of merit ZT value comparing the other alloy for the reason that the maximum ZT value is 0.85, which is achieved by the n-doped material (n-type semiconductor) with an optimal carrier concentration of $-3.5 \times 10^{19}\ Cm^{-3}$ whereas for a p-type semiconductor, the highest ZT value is around 1.024 with carrier concentration $n = 6.16 \times 10^{19}\ Cm^{-3}$ for the $ScTaPt_2Sn_2$ alloy (see table 11).

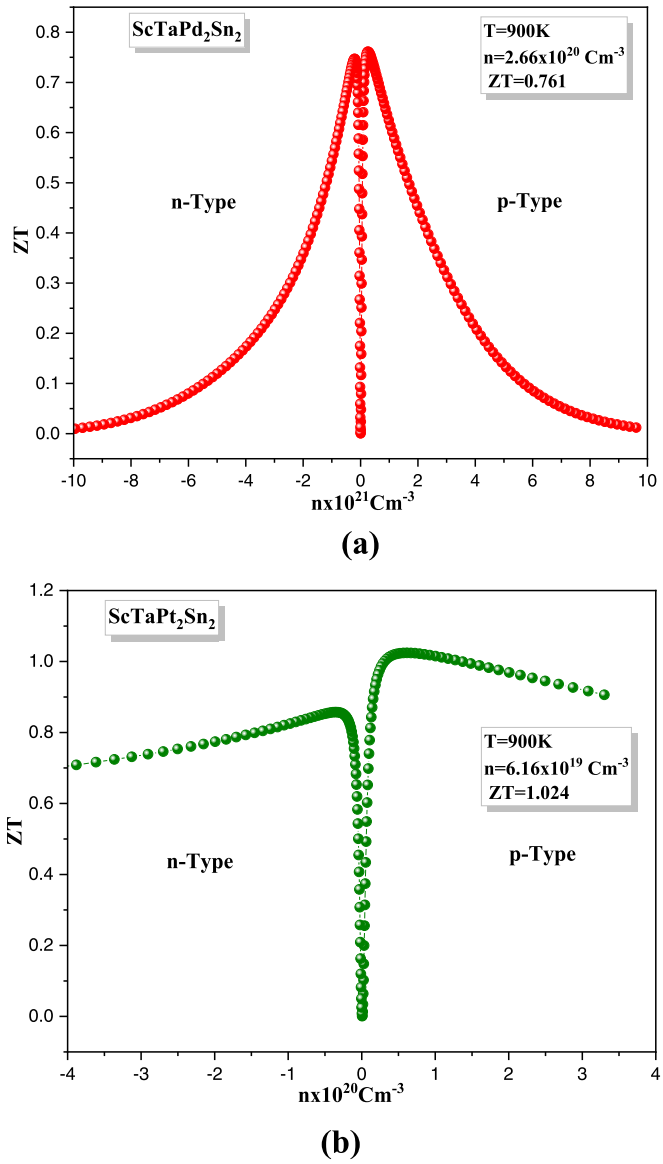

Figure 17. The figure of merit ZT of the DHH alloys (a) $ScTaPd_2Sn_2$ and (b) $ScTaPt_2Sn_2$ as a function of charge carrier concentration at fixed temperature T = 900 K.

Table 11. Calculated ZT and corresponding transport coefficient at the optimal chemical potential for the DHH alloys $ScTaPd_2Sn_2$, and $ScTaPt_2Sn_2$ at various temperatures.

Alloys	μ (eV)	T(K)	n(Cm^{-3})	K_e (W/m.K)	σ ($10^5/\Omega$.m)	S (μV/K)	ZT
$ScTaPd_2Sn_2$	0.68326	1000	6.82×10^{20}	23.46	3.8428	206.81	0.664
		900	5.84×10^{20}	19.07	3.4159	209.7	0.658
		300	1.55×10^{20}	1.72	1.2148	173.8	0.16
	0.68866	900	2.66×10^{20}	13.67	1.6281	267.08	0.761
	0.68806	900	2.91×10^{20}	14.23	1.7694	260.7	0.69
$ScTaPt_2Sn_2$	0.74039	1000	4.02×10^{20}	14.854	2.1765	245.99	0.816
		900	3.35×10^{20}	11.6	1.922	246.26	0.803
		300	9.8×10^{19}	1.01	8.67745	138.72	0.083
	0.74709	1000	1.67×10^{20}	9.56	0.94888	313.73	0.861
	0.75149	900	6.16×10^{19}	4.81	0.3871	376.36	1.024

Hence, the double half Heusler alloy discussed in our study is considered the most suitable material for thermoelectric applications, primarily due to its high figure of merit, a crucial parameter in the field of thermoelectricity.

4. Conclusion

In this research, a theoretical investigation of $ScTaPd_2Sn_2$ and $ScTaPt_2Sn_2$ a new DHH were carried out using Wien2k code, which included several properties such as structural, electronic, optical, elastic and thermoelectric. Based on the obtained calculations, it is evident that our compounds have characteristics of a semiconductor and possesses an indirect band gap. Additionally, the determination of the density of states demonstrates that the d orbitals have the most substantial contribution to the overall density of states. The optical spectra, including the dielectric function, refractive index, and extinction coefficient, exhibit similarities to $ScNbNi_2Sn_2$. The analysis of the elastic characteristics suggests that our compounds exhibit stability. The thermoelectric characteristics of our compounds indicate that $ScTaPd_2Sn_2$ and $ScTaPt_2Sn_2$ exhibit moderate thermoelectric efficiency

Acknowledgments

The authors (H Mekki, H Baaziz, Z Charifi, and T Ghellab) would like to thank the general directorate for scientific research and technological development for their financial support during the realization of this work.

Data availability statement

No new data were created or analysed in this study.

ORCID iDs

H Baaziz https://orcid.org/0000-0003-4860-2740
Z Charifi https://orcid.org/0000-0003-3875-4716

References

[1] Anand S, Wood M, Xia Y, Wolverton C and Snyder G J 2019 *Joule* **3** 1226–38
[2] Mekki H, Baaziz H, Charifi Z, Ghellab T, Genç A and Uğur G 2023 *Solid State Commun.* **363** 115103
[3] Ugur G, Kushwaha A K, Güler M, Charifi Z, Ugur S, Güler E and Baaziz H 2022 *Materials Science in Semiconductor*
[4] Charifi Z, Baaziz H, Ugur S and Ugur G 2022 *Indian J. Phys.* **97** 413
[5] Slamani A, Khelfaoui F, Sadouki O, Bentayeb A, BoudiaK and Belkharroubi F 2023 *Emergent Materials* **6** 681–90
[6] Rached Y, Caid M, Merabet M, Benalia S, Rached H, Djoidi L, Mokhtari M and Rached D 2022 *Int. J. Quantum Chem.* **122**
[7] Sahni B and Alam A 2023 arXiv:2301.00598
[8] Rabin D, Fuks D and Gelbstein Y 2023 *Phys. Chem. Chem. Phys.* **25** 520–8
[9] Anand S, Xia K, I. Hegde V, Aydemir U, Kocevski V, Zhu T, Wolverton C and Snyder G J 2018 *Energy Environ. Sci.* **11** 1480
[10] Blaha P, Schwarz K, Madsen G K H, Kvasnicka D and Luitz J 2001 *WIEN2k, an Augmented Plane Wave Plus Local Orbitals Program for Calculating Crystal Properties, Vienna University of Technology*
[11] Blaha P, Schwarz K, Tran F, Laskowski R, Madsen G K H and Marks L D 2020 *J. Chem. Phys.* **152** 074101
[12] Kohn W and Sham L J 1965 *Phys. Rev.* **140** A1133–8
[13] Hohenberg P and Kohn W 1964 *Phys. Rev.* **136** B864
[14] Perdew J P, Burke K and Ernzerhof M 1996 *Phys. Rev. Lett.* **77** 3865
[15] Perdew J P and Wang Y 1992 *Phys. Rev.* B **45** 13244–9
[16] Tran F and Blaha P 2009 *Phys. Rev. Lett.* **102** 226401
[17] Engel E and Vosko S H 1993 *Phys. Rev.* B **47** 13164
[18] Madsen G K H and Singh D J 2006 *Comput. Phys. Commun.* **175** 67
[19] Otero-de-la-Roza A 2011 Gibbs2: a new version of the quasi-harmonic model code. I. Robust treatment of the static data *Comput. Phys. Commun.* **182** 1708–20
[20] Anand S, Xia K, Hegde V I, Aydemir U, Kocevski V, Zhu T, Wolverton C and Snyder G J 2018 A valence balanced rule for discovery of 18-electron half-Heuslers with defects *Energy Environ. Sci,* **11** 1480–8
[21] Murnaghan F D 1944 *Proc. Natl Acad. Sci.* **30** 244
[22] Kramers H A 1927 *Atti Cong. Intern. Fisica (Transactions of Volta Centenary Congress, Como).* **2** 545–57
[23] Jamal M, Bilal M, Ahmad I and Jalali-Asadabadi S 2018 *J. Alloys Compd.* **735** 569
[24] Hill R 1952 The elastic behaviour of a crystalline aggregate *Proc. Phys. Soc.* A **65** 349–54
[25] Tao X, Yang J, Xi L and Ouyang Y 2012 First-principles investigation of the thermo-physical properties of Ca3Si4 *J. Solid State Chem.* **194** 179–87
[26] Mao P, Yu B, Liu Z, Wang F and Ju Y 2015 First-principles investigation on mechanical, electronic, and thermodynamic properties of Mg2Sr *under high pressure. J. Appl. Phys.* **117** 115903
[27] Voigt W 1928 *Lehrbuch der Kristallphysik; Taubner: Leipzig*
[28] Reuss A 1929 Calculation of the flow limits of mixed crystals on the basis of the plasticity of monocrystals *Z. Angew. Math. Mech.* **9** 49–58
[29] Ravindran P, Fast L, Korzhavyi P A and Johansson B 1998 *J. Appl. Phys.* **84** 4891
[30] Pugh S F 1954 *Philos. Mag.* **45** 823
[31] Bao L, Qu D, Kong Z and Duan Y 2019 *Solid State Sci.* **98** 106027

[32] Luo X and Wang B 2008 Structural and elastic properties of LaAlO 3 from fi rstprinciples calculations *J. Appl. Phys.* **104** 073518–24
[33] Anderson O L (ed) 1963 A simplifi ed method for calculating the debye temperature oborobofrom elastic constants *J. Phys. Chem. Solids* **24** 909–17
[34] Schreiber E, Anderson O L and Soga N 1973 *Elastic Constants and their Measurements* , *McGraw-Hill*
[35] Ravindran P, Fast L, Korzhavyl P A, Johansson B, Wills J and Eriksson O 1998 *J. Appl.Phys.* **84** 4891
[36] Chung D H and Buessem W R 1968 *Proceedings* (Plenum Press)
[37] Ranganathan S and Ostoja-Starzewski M 2008 *Phys. Rev. Lett.* **101** 055504–7
[38] Nye J F 1957 *Physical Properties of Crystals: Their Representation by Tensors and Matrices* (Oxford University Press)
[39] Slack G A 1973 *J. Phys. Chem. Solids* **34** 321
[40] Shinde S L and Goela J 2006 *Condens. Matter Phys. XVIII* **271** 133
[41] Blanco M A, Francisco E and Luaña V 2004 *Comput. Phys. Commun.* **158** 57 Source code distributed by the CPC program library: http://cpc.cs.qub.ac.uk/
[42] Toher C *et al* 2014 *Phys. Rev.* B **90** 174107
[43] Blanco M *et al* 1996 *J. Mol. Struct. Theochem.* **368** 245
[44] Poirier J-P 2000 *Introduction to the Physics of the Earth's Interior* (Cambridge University Press)
[45] Mili I, Latelli H, Charifi Z, Baaziz H and Ghellab T 2022 *Comput. Mater. Sci.* **213** 111678
[46] Zheng J-C 2008 *Front. Phys. China* **3** 269
[47] Nag B R 1980 *Electron Transport in Compound Semiconductors* (Springer) 171 {229
[48] Scheidemantel T J *et al* 2003 *Phys. Rev.* B **68** 125210
[49] Thonhauser T *et al* 2003 *Phys. Rev.* B **68** 085201
[50] Kim H *et al* 2015 *APL Mater.* **3** 041506
[51] Ahmad Khandy S, Kaur K, Dhiman S, Singh J and Kumar V 2021 *Comput. Mater. Sci.* 188
[52] Liechtenstein A I, Vladimir I A and Jan Z 1995 *Phys. Rev.* B **52** R5467